OPTICAL INTERFERENCE PHENOMENON

C. W. von Rosenberg, Jr., et al

Avco Everett Research Laboratory

Prepared for:

Defense Nuclear Agency

February 1974

UNCLASSIFIED

SECURITY CLASSIFICATION OF THIS PAGE (When Data Entered)

REPORT DOCUMENTATION PAGE		READ INSTRUCTIONS BEFORE COMPLETING FORM
1. REPORT NUMBER DNA-3239F	2. GOVT ACCESSION NO.	3. RECIPIENT'S CATALOG NUMBER AD-782 275
4. TITLE (and Subtitle) OPTICAL INTERFERENCE PHENOMENON		5. TYPE OF REPORT & PERIOD COVERED Final Report 1 Sept 1971 - 31 July 1973
		6. PERFORMING ORG. REPORT NUMBER
7. AUTHOR(s) C. W. von Rosenberg, Jr., Daniel W. Trainor, and Andrew Lowenstein		8. CONTRACT OR GRANT NUMBER(s) DNA 001-72-C-0007
9. PERFORMING ORGANIZATION NAME AND ADDRESS Avco Everett Research Laboratory 2385 Revere Beach Parkway Everett, Mass. 02149		10. PROGRAM ELEMENT, PROJECT, TASK AREA & WORK UNIT NUMBERS ARPA Order No. 1433, Amend 2, 4 & 7, Task No. 1E50, 2E50 &3E50, Work Unit No. 04 & 07
11. CONTROLLING OFFICE NAME AND ADDRESS Director Defense Nuclear Agency Washington, D.C. 20305		12. REPORT DATE February 1974
		13. NUMBER OF PAGES 83
14. MONITORING AGENCY NAME & ADDRESS(if different from Controlling Office)		15. SECURITY CLASS. (of this report) Unclassified
		15a. DECLASSIFICATION DOWNGRADING SCHEDULE

16. DISTRIBUTION STATEMENT (of this Report)

Approved for public release; distribution unlimited.

17. DISTRIBUTION STATEMENT (of the abstract entered in Block 20, if different from Report)

18. SUPPLEMENTARY NOTES

This work was supported by the Nuclear Defense Agency under Subtask ZL433-07.

19. KEY WORDS (Continue on reverse side if necessary and identify by block number)

Reaction rate studies
Ozone formation
Chemiexcitation
Vibrational relaxation
Absorption studies
Atmospheric chemistry

20. ABSTRACT (Continue on reverse side if necessary and identify by block number)

Experimental measurements of the formation of vibrationally excited ozone resulting from $O + O_2 + M \rightarrow O_3^{\dagger} + M$, $M = C_2$, N_2 are reported. The bulk rate constant and the exothermicity of the reaction going into various vibrational states of ozone are given. The rate for vibrational relaxation $O_3^{\dagger} + M \rightarrow O_3 + M$ was also measured. Separate experiments on the absorption of CO_2 9.6μ laser lines by ozone are described as well as a measurement of CO_2 (ν_3) relaxation by ozone.

DD FORM 1 JAN 73 1473 EDITION OF 1 NOV 65 IS OBSOLETE

UNCLASSIFIED

SECURITY CLASSIFICATION OF THIS PAGE (When Data Entered)

ABSTRACT

Experimental measurements of the formation of vibrationally excited ozone resulting from $O + O_2 + M \rightarrow O_3^{\dagger} + M$, $M = O_2, N_2$ are reported. The bulk rate constant and the exothermicity of the reaction going into various vibrational states of ozone are given. The rate for vibrational relaxation $O_3^{\dagger} + M \rightarrow O_3 + M$ was also measured. Separate experiments on the absorption of CO_2 9.6μ laser lines by ozone are described as well as a measurement of CO_2 (ν_3) relaxation by ozone.

TABLE OF CONTENTS

LIST OF ILLUSTRATIONS

1.0 INTRODUCTION

This report contains a rather complete description of the major accomplishments on this program without dwelling on all of the details and difficulties along the way. It is anticipated that Section 2.0 on vibrational excitation of ozone formed by recombination will sometime be submitted to DNA, with minor changes, for public release and publication in the open literature. The major accomplishments in this part were the clear observation of vibrational excitation, and IR emissions therefrom, in both the ν_3 and ν_2 modes. Quantitative reduction allowed us to determine quantitatively the rate of recombination for $O + O_2 + O_2 \rightarrow O_3 + O_2$, the rate of vibrational relaxation for $O_3^{\dagger} + O_2 \rightarrow O_3 + O_2$, and the average number of quanta formed per recombination for the three normal modes of ozone vibration. Emission from high vibrational levels of the ν_3-mode was observed and is discussed and the effect of N_2 on these processes was determined.

Section 3.0 deals with a task whose requirement was to determine if a CO_2 laser could be used to excite ozone in a laser fluorescence experiment to measure the vibrational relaxation of ozone. We measured the previously unknown cross sections for absorption of CO_2 laser lines by ozone and calculated that such a fluorescence experiment could be performed. Before this phase of the contract expired an initial attempt was made to measure the relaxation of ozone, but was unsuccessful. We did determine the (previously unknown) rate for vibrational relaxation of CO_2 (ν_3) by ozone. By the time of the follow-on our photolysis apparatus was giving excellent data from which it had become apparent (somewhat surprisingly) that the relaxation of ozone was sufficiently slow that it could also be measured. It was not proposed therefore to continue the fluorescence studies but rather to concentrate on the photolysis experiments.

2.0 VIBRATIONAL EXCITATION OF OZONE FORMED BY RECOMBINATION

C. W. von Rosenberg, Jr. and Daniel W. Trainor

2.1 INTRODUCTION

There is considerable interest in vibrational excitation resulting from simple chemical reactions, and much current work in chemical kinetics is directed toward understanding under what conditions it occurs. For the particular case of recombination reactions, theories have long utilized a mechanism whereby recombination occurs leaving the nascent molecule in its highest vibrational levels with subsequent stabilization occurring by cascading down the vibrational ladder to the lower levels by radiative and collisional quenching processes. Such a recombination mechanism assures vibrational excitation and for processes of the sort $A + B + M \rightarrow AB + M$, the mechanism is relatively easy to visualize and there is some experimental evidence to substantiate the picture.[1] For the formation of triatomics by reactions of the sort $AB + C + M \rightarrow ABC + M$ the process is more complicated, since there is more than one vibrational mode in which the bond energy may be deposited. In the absence of any prevailing theory, experimental evidence concerning the proportioning of recombination energy among the normal modes should be particularly valuable in understanding these processes.

Earlier experimental studies on the particular recombination of $O + O_2$ to form $O^{\dagger}_3$ have utilized UV absorption of the Hartley band as the principal diagnostic. By obtaining measurements at several wavelengths as a function of time after pulsed formation of O-atoms (by either radiolysis or flash photolysis of O_2) Hochanadel, Ghormley, and Boyle: HGB[2] observed a temporal dependence in the spectral profile of the band. They interpreted this as being due to vibrational excitation in the ozone formed by recombination. Analysis of their data gave values for the recombination rate and for vibrational relaxation of $O^{\dagger}_3$. Similar work by Riley and Cahill[3] takes issue with the HGB interpretation and suggests some "transient species," that is

not vibrationally excited ozone, may be responsible for the transient portion of the UV absorption in their work and the HGB work. Subsequently, in quite similar studies, Bevan and Johnson[4] studied the kinetics of ozone formation following pulse radiolysis of oxygen. They observed two transient features in their spectral band shape measurements which they attributed to two species they labeled as O_3^{α} and O_3^{β}, which they suggest are probably vibrationally excited ozone.

In the present work we perform similar experiments with the important difference being our use of IR detection. By observing emission at 9.6 and 14.3μ we are able to answer the question directly; i.e., there is vibrational excitation in at least the ν_3 and ν_2 modes of ozone and we quantitatively report the mean degree of excitation in these modes resulting from recombination. We also obtain data on the vibrational relaxation of ozone and on the net recombination rate. A preliminary discussion of this work has been published.[5]

2.2 EXPERIMENTAL

The experimental apparatus is shown to scale in Figure 1. Its outer envelope is a quartz cylinder (13 cm dia.) painted black on its inside surface to reduce stray reflections. Four normal quartz linear flashlamps (Xenon Corp. modified model FP-6) are wired as two parallel pairs of two lamps in series; they are pulsed by a 16μf capacitor bank operating at 7 to 14 kV (600 J is typical). The UV light emission from the lamps was measured and found to have an 8μsec full width at half peak and a time to 98% extinction of 32μsec (the shape is plotted at the lower right of Figure 11). In our development of the apparatus we found that one source of stray IR light was thermal emission from the hot flashlamp tube. This was eliminated by filtering with a quartz tube around each flashlamp and another quartz tube surrounding the center axis of the test cell; see Figure 1. There was no direct pick-up of flashlamp output since quartz does not transmit at wavelengths longer than 4μ and the IR filters did not transmit at wavelengths shorter than 7.5μ.

The two diagnostics used were 2537 Å UV absorption and IR detection. The UV absorption measurements were strictly for obtaining ozone concentrations before and after kinetic processes had occurred. The UV system measurements utilized an RCA-1P28 photomultiplier (PM) and a

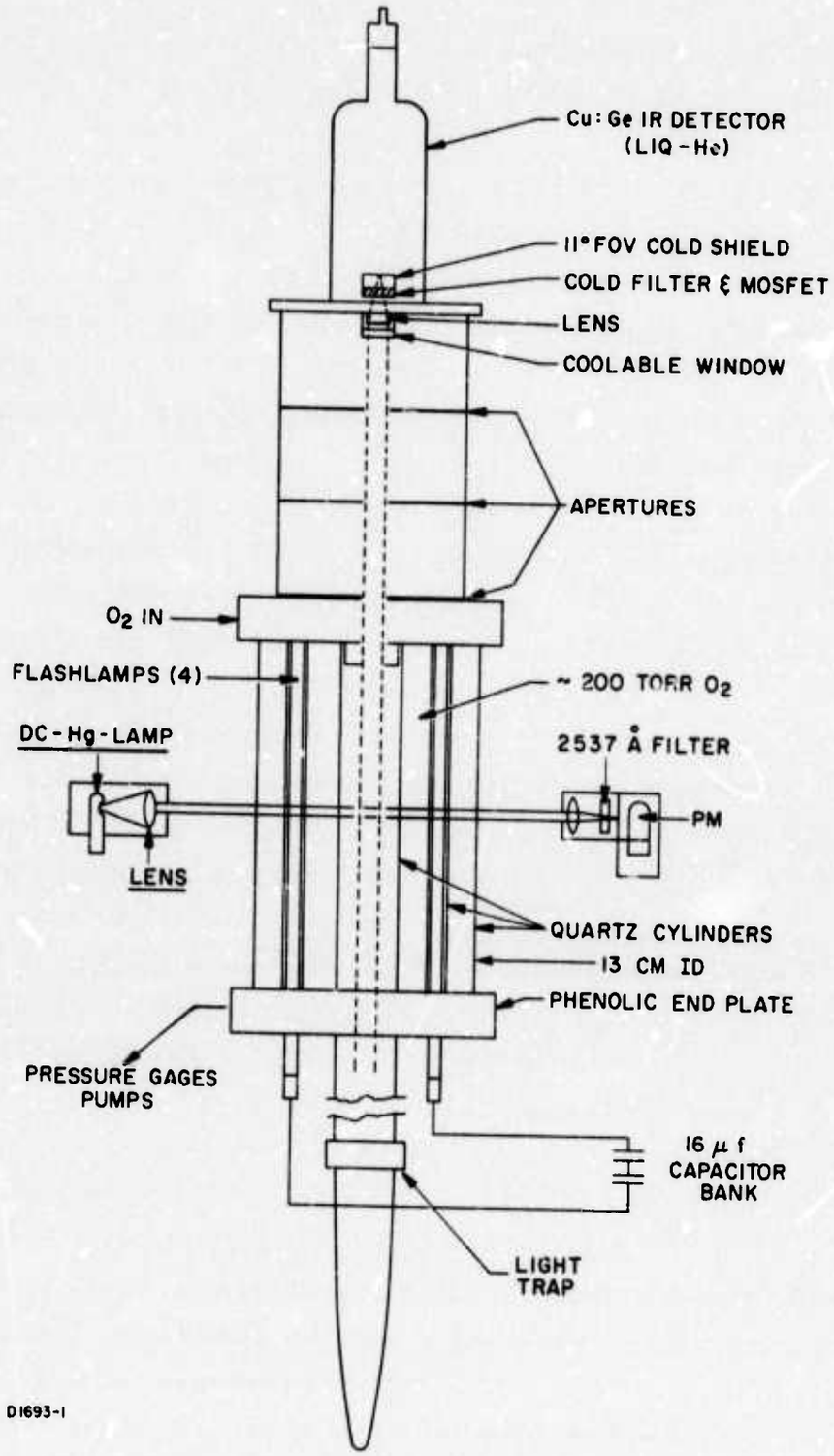

Figure 1 Scale Drawing of Experimental Apparatus with IR Detection and UV Absorption Diagnostics

low pressure mercury discharge lamp of the sort commonly used for spectrograph calibrations (Edmund Scientific No. 40759) but operated DC ultimately, an Osram HB O 100 W/2 DC mercury arc lamp was used. Being a higher pressure device it had a rather broad 2537 Å emission which we investigated with a monochromator/PM. To limit our measurement near the Hartley band peak an additional 2537 Å filter was used in the optical path and a specific calibration was performed with known amounts of O_3 to allow relating UV absorption to $[O_3]$ when Beer's law was invalid due to the non-monochromatic source and spectrally dependent absorption of O_3. All of our measurements of $[O_3]$ by 2537 Å absorption were performed only on vibrationally relaxed (ground state) ozone. The measurements were performed in two ways: 1) transverse to the cell axis as shown in Figure 2, and 2) along the cell axis by replacing the IR detector with a quartz window plus the Hg-light source and replacing the bottom light trap with a window plus PM. In the latter case data are reduced under the assumption that ozone photolysis only occurs between the two phenolic end plates and that apertures prevent appreciable flashlamp light from entering the upper chamber (with apertures) or the long tube leading to the lower light trap. If this assumption is in error it is canceled in the quantitative reduction of our IR data since the same viewing path is used, the same assumption is applied, and only a small degree of IR self-absorption occurs.

The IR detector is a Cu:Ge liquid helium cooled device (custom built for this experiment by Santa Barbara Research Center) which vacuum seals directly to the top of the test cell and views down its center axis through a series of light baffles in a copper enclosure. The detector contains an 11° field-of-view cold shield, appropriate filter (Optical Coating Lab., Inc.) Irtran IV lens (Kodak), bias resistor, and MOSFET preamplifier all cooled to 5°K. Extensive electrical shielding light baffling and optical filtering were a major part of the development that now allows us to view background limited (300°K) IR signals at 10μ as early as 10-20μsec after initiation of the flash with 3.25μsec time resolution thereafter. Both the detector's Irtran window and the light trap into which the detector viewing terminates are coolable to liquid nitrogen temperature in order to obtain lower background noise and higher sensitivity, but this additional complication has not been necessary.

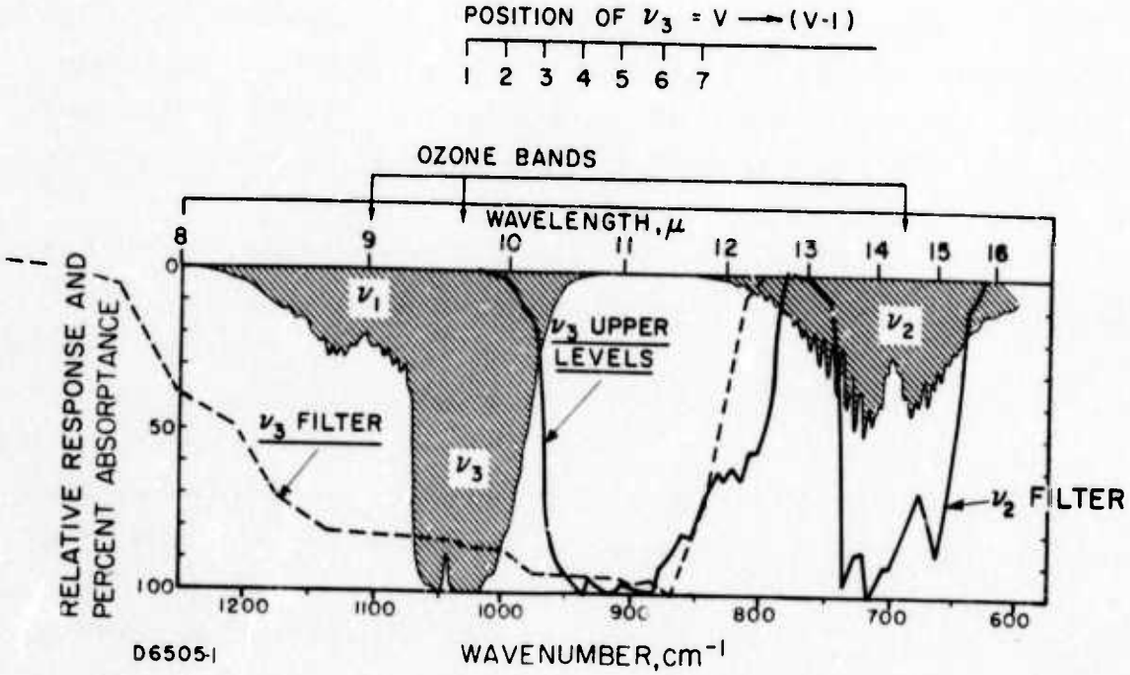

Figure 2 Room Temperature Absorption Spectrum of Ozone as Given by McCaa and Shaw Overlayed with the Detection System's Relative Spectral Response for Three Different Filters used in this Work. Filters are labeled: (a) ν_3-band, (b) ν_3-upper levels, and (c) ν_2-band. The change in the ν_3-band center for higher transitions ($v = 2 \rightarrow 1$, $3 \rightarrow 2$, etc.) due to anharmonicity is indicated; based on the work of McCaa and Shaw.[6]

Since the spectral transmission function of an interference filter varies with temperature, we measured the net spectral response of the detector with cold filter and lens installed by scanning a standard "blackbody" radiation source with a monochromator of known spectral response and dispersion. The resulting normalized net response of the system is shown in Figure 2 for the three filters used in this work along with the room temperature absorption spectrum of ozone from McCaa and Shaw.[6] By far the largest quantity of our data has been taken with the "ν_3-band" filter and except when otherwise stated it may be assumed that this was the filter in use.[†]

For our quantitative measurements of radiation we calibrated the detector by utilizing the difference in emission of a room temperature chopper and an ice temperature "blackbody." The chopper radiation is due to its own emission and reflection of radiation from the room and since they are at the same temperature it radiates like a blackbody at that temperature. The ice cooled blackbody is a cavity of blackened copper walls kept in an ice + water slurry at 0°C. This pair of reference sources allows us to generate AC signals of sufficiently small magnitude that the detector is not saturated and operates at a signal level comparable to that obtained in the experiment. We measured a $D^* = 9.9 \times 10^{10}$ watt^{-1} Hz$^{1/2}$ cm with the ν_3-band filter installed (Cu:Ge crystal impedance = 5.3×10^6 ohms). The detector system time response was measured by exposing it to scattered radiation from a Q-switched N_2-CO_2 laser. The detector had an exponential recovery with a time constant of 3.25μsec.

The experimental design was to operate at pressures around 200 torr in pure O_2. By use of normal quartz flashlamps, there should be very few photons transmitted below 1760 Å. Since singlet state $O(^1D)$ is only obtained for $\lambda \leq 1759$ Å,[7] we utilized the long wavelength edge of the O_2 Schumann-Runge absorption band to obtain ground state O-atoms by

[†] Our "ν_3-band" filter encompasses the ν_1-mode but is interpreted as responding only to ν_3-emissions since the radiative lifetime of the ν_1-mode is 30-fold larger than for the ν_3-mode and since, as will be discussed, the two modes are assumed in equilibrium with each other.

$$O_2 + h\nu\ (\lambda \gtrsim 1760\ \text{Å}) \rightarrow O(^3P) + O(^3P).$$

We were concerned that if $O(^1D)$ were produced it would complicate the interpretation since even though it would quench in a few collisions with O_2 it would generate $O_2\ (^1\Sigma)$ and/or vibrationally excited O_2 in the process[8-10] which could subsequently pump the ozone by collisional energy transfer.

At around 200 torr with small O-atom production, the fate of virtually all O-atoms formed is to recombine via

$$O(^3P) + O_2 + O_2 \rightarrow O_3 + O_2 \qquad (1)$$

and form an ozone molecule. Therefore by measuring $[O_3]$ after a flash in pure O_2 one has a measure of [O] generated by the flash. Measurements along the cell axis shown in Figure 3 demonstrate that we make about 7.8×10^{-5} mole fraction of [O] in a single flash. At 200 torr and below this fraction is constant with pressure, presumably because the gas is optically thin even at the wavelength of the maximum absorption. At 400 torr the fraction has decreased due to the photon absorption length becoming comparable to the cell dimensions; i.e., at 400 torr a higher fraction of O_2 is photolyzed adjacent to the flashlamps than is photolyzed in the middle of the cell. This interpretation is reasonable since the wavelength for highest photolysis efficiency should be the wavelength where the product of quartz transmission and O_2-absorption coefficient is a maximum, or near 1800 Å and for this wavelength the absorption coefficient of $\alpha \simeq 1\ \text{cm}^{-1}\ \text{ama}^{-1}$[7] gives an absorption length of $\ell = (\alpha n_{O_3})^{-1} = 1.9$ cm at 400 torr; the distance from the flashlamps to the cell axis is 3.3 cm.

In this work, high purity O_2 was used with a manufacturers (Air Reduction-AIRCO) stated purity of Xe = 1 ppm, N_2 = 4, Ar = 10.2, and Kr = 12 ppm with a balance of O_2. Some runs with normal cylinder O_2 were also used with no effect on the data.

In order to improve our O-atom concentration and therefore our signals we used ozone plus oxygen mixtures (0.3% O_3 + O_2 typically) for most of our data. There are possible kinetic complications due to the Hartley band photolysis of O_3

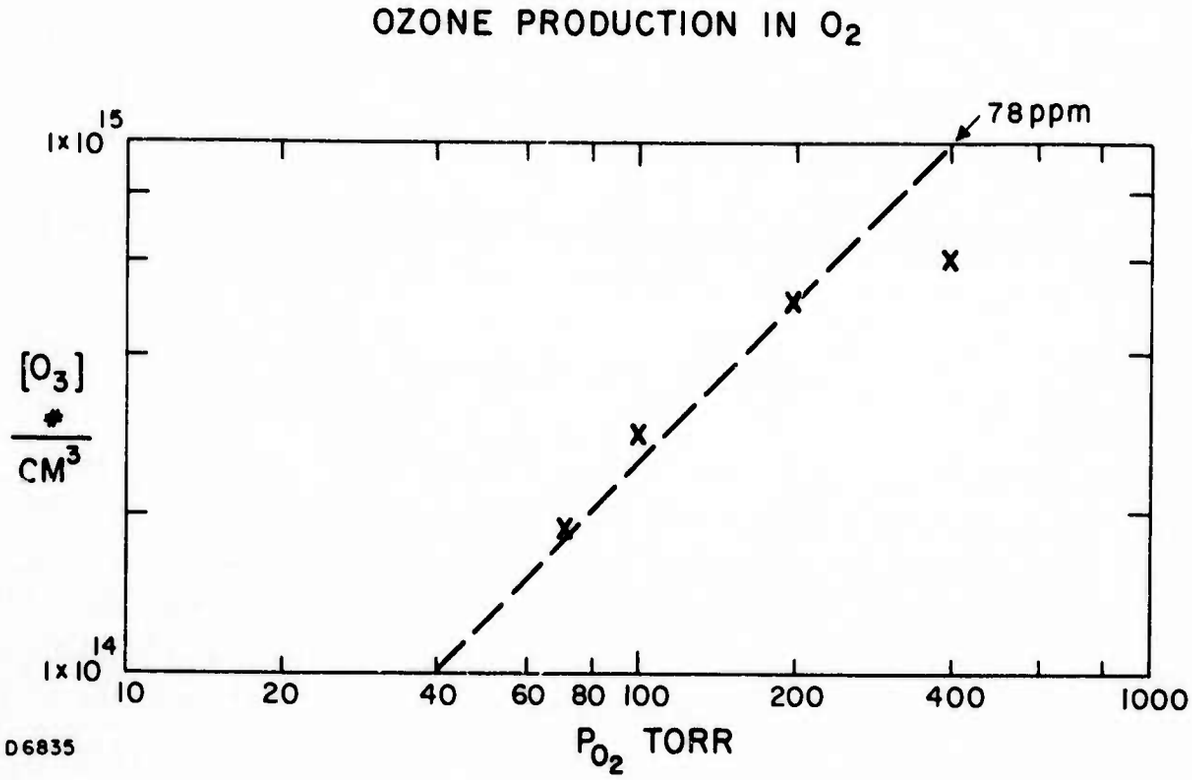

Figure 3 Production of $[O_3]$, and hence $[O]$, along the Axis of Symmetry (IR Viewing Axis) for Flashes of 580 J in Pure O_2 in Our System

$$O_3 + h\nu\ (\lambda \sim 2500\ \text{Å}) \rightarrow O(^1D) + O_2\ (^1\Delta)$$

giving excited states of O and O_2.[7-11] This has been discussed in part already but will be treated more completely later where we show that the excited states do not interfere with our measurements of Reaction (1).

The ozone used in these experiments was generated in a discharge, distilled by trapping at liquid N_2 temperature, and pumped on to preferentially remove O_2. A high purity stainless steel mixing tank with a magnetically driven stirrer was used for the ozone plus oxygen and/or nitrogen mixes.

The photolysis apparatus would pump to below 1μ with pumping through a 100 cm 3/8 inch copper tubing connecting to a 2 inch liquid N_2 trapped oil diffusion pump (Varian DC 704 pumping fluid). Mechanical pumps were used with Fyrquel 220 Triaryl phosphate (Stauffer Chemical Co.) oil to prevent any explosion when pumping pure O_2; mixing of N_2 with the O_2 before entering the pump was another precaution we used for safety. Mixtures with appreciable ozone were pumped through a canister filled with soda lime to decompose the ozone.

2.3 THEORY

The experiments are basically performed under conditions where the time scales of interest are related by

$$\tau_d < \tau_v < \tau_r,$$

where τ_d = duration of the flashlamp discharge ($\sim 8\mu$sec), τ_v = vibrational relaxation of ozone (~ 20 to 70μsec), and τ_r = recombination time (~ 20 to 300μsec). The temporal behavior of the IR signals can be anticipated by using the following two-level model which is the simplest model that has the essential features of the kinetics:

$$O + O_2 + O_2 \xrightarrow{(1-\phi)k_1} O_3\ (v=0) + O_2 \qquad (1a)$$

$$\xrightarrow{\phi k_1} O_3\ (v=1) + O_2 \qquad (1b)$$

$$O_3 (v = 1) + O_2 \xrightarrow{k_2} O_3 (v = 0) + O_2 \qquad (2)$$

In these reactions only one vibrational mode is mentioned; it of course would be the one responsible for the IR radiation seen by the detector. A more complete analysis would recognize the existence of all three modes, the various levels of each mode, intramolecular vibration-vibration (V-V) transfer within a single mode and between modes of ozone for collisions with either O_2 or other O_3, and intermolecular V-V transfer with the O_2 as well as the translation-vibration (T-V) transfer listed. Clearly if this model is used to reduce the data the values obtained for k_1, k_2 and ϕ will have a deeper meaning than is implied by Reactions (1) and (2). In this model k_1 is the net recombination rate regardless of any vibrational excitation in the product and it should be comparable to literature values.[12-16] The parameter ϕ is the fraction of the recombination that goes into channel (2b). In the broader sense ϕk_1 is the rate of ozone excitation in the mode of interest expressed as quanta per cm^3 per sec. If every recombination gave $v = 1$ then $\phi = 1$ would explain the data; if half of the recombinations gave $v = 2$ and the other half $v = 0$ and there were a rapid V-V shuffle of the type

$$O_3 (v = 2) + O_3 (v = 0) \rightarrow O_3 (v = 1) + O_3 (v = 1)$$

then the data would still give $\phi = 1$. If all recombinations gave $v = 2$ and no V-V shuffling occurred and the rate for

$$O_3 (v = 2) + O_2 \xrightarrow{k_3} O_3 (v = 1) + O_2 \qquad (3)$$

was $k_3 = k_2$, then upon reduction the data would yield $\phi = 2$.

The relaxation rate k_2 is expressed as a simple T-V process in which quanta are lost forever from the mode of interest. If for example the mode of interest is ν_3 and the processes

$$O_3 (\nu_3 = 1) + O_2 \rightarrow O_3 (\nu_2 = 1) + O_2 + KE$$

and/or

$$O_3 (\nu_3 = 1) + O_2 \rightarrow O_3 (\nu_3 = 0) + O^{\dagger}_2$$

dominate, then observations of the ν_3-mode emission will not know the difference and the value deduced for k_2 may in fact represent a V-V rather than a T-V rate.

More complicated models will be considered later, but for the moment the use of Eqs. (2) and (3) will suffice. Together they imply

$$\frac{d}{dt} [O_3 (v=1)] = \phi k_1 [O] [O_2]^2 - k_2 [O_3 (v=1)] [O_2] \qquad (4)$$

which, together with the appropriate boundary conditions, has the solution:

$$[O_3 (v=1)] = \phi \frac{R_1 [O]_o}{R_2 - R_1} \left\{ e^{-R_1 t} - e^{-R_2 t} \right\} \qquad (5)$$

where $R_1 = k_1 [O_2]^2$ and $R_2 = k_2 [O_2]$. The initial boundary conditions were taken as $[O] = [O]_o$ at flash initiation with no subsequent production of O-atoms, and $[O_3 (v=1)] = 0$. This is not always valid for our data since although τ_d is less than τ_v or τ_r it is of comparable size at the higher pressures, and it is not a delta function but is distributed in time. Nevertheless, Eq. (5) has considerable utility for understanding the data. It predicts a temporal behavior controlled by the difference in two exponentials; for our work $R_2 > R_1$ so the signal shape is as illustrated in Figure 4. This shape is completely independent of the value of ϕ; however the overall magnitude scales with ϕ (and $[O]_o$). A little reflection on Figure 4 shows that if R_2 is much larger than R_1 then the time to the peak is essentially related to R_2 and should scale inversely with k_2 and $[O_2]$ or total pressure. Further, the final signal decay is basically exponential with a characteristic time of $1/R_1$ so that k_1 may be deduced from this part of the data. The simplest statement of the late time behavior is the solution of Eq. (4) under conditions of quasi-steady state obtained by setting $d [O_3 (v=1)]/dt = 0$ giving

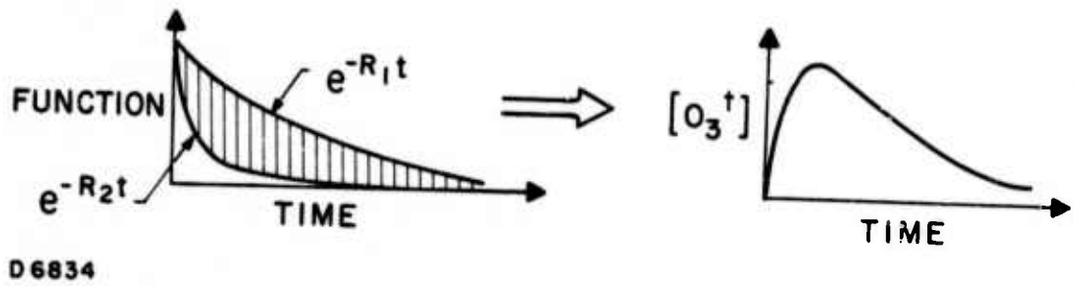

Figure 4 Expected Temporal Behavior of Our IR Signals as Controlled by the Difference of the Two Exponentials in Eq. (5). Early time behavior is controlled by the vibrational relaxation rate R_2 and late time behavior by the recombination rate R_1.

$$[O_3 (v = 1)] = \phi \frac{k_1}{k_2} [O] [O_2].$$

Since $[O] = [O]_o e^{-R_1 t}$ it is clear that $[O_3 (v = 1)]$ (and thus the IR emission) has this same temporal behavior.

For convenience in reducing the data an expression for the time of maximum signal, t_{max}, is obtained by using Eq. (5) and

$$\frac{d [O_3 (v = 1)]}{dt} = 0 \text{ at } t = t_{max}$$

to obtain

$$t_{max} = \frac{3.1 \times 10^{-11}}{p k_2} \frac{\ln R}{(R - 1)} \qquad (6)$$

where $R = R_1/R_2$, t = μsec, p = torr, and $k_2 = cm^3 sec^{-1}$. This equation is used for obtaining k_2 and Eq. (5) is used for obtaining ϕ from the data.

2.4 RESULTS

2.4.1 Oscillograms O_2 and $(O_3 + O_2)$

In Figure 5 we display runs in pure N_2 and pure O_2. There is an initial sweep of about 3.5μsec, firing of the flashlamps producing electrical noise on the signal for about 10μsec during the discharge, and then valid measurements o IR emission. No emission is expected in pure N_2, and it serves for comparison. In fact, a very small increase in signal level is observed in the N_2 trace and we attribute it to scattered thermal photons from the flashlamp envelope or from surfaces heated by absorption of visible photons. It was considerably larger without the quartz envelope around the flashlamps or around the central axis of the photolysis cell (see Figure 1). The signal from pure O_2 shows the expected behavior: a rise to a maximum, and then a decay.

In Figure 6 we show a run in O_2 + 0.31% O_3. The $[O]_o$ is an order of magnitude larger here than in Figure 5 so that the signal-to-noise (S/N) is much better and one can see the temporal behavior quite clearly. It is just as expected except for the slightly sigmoid appearance of the approach

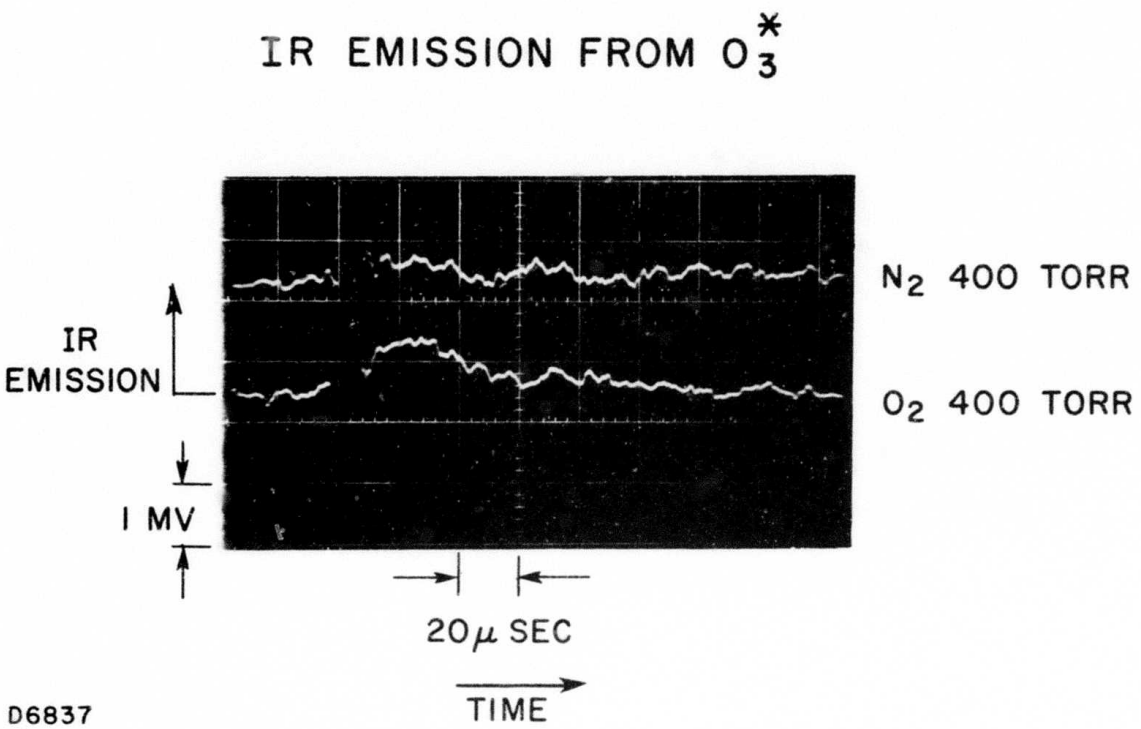

Figure 5 Oscillograms Showing IR Emission from $O_3^{\dagger}$, Vibrationally Excited Ozone (ν_3-Band Filter) Formed from Flashes in Pure O_2 Compared to the Nil Signal Expected in Pure N_2 Experiments

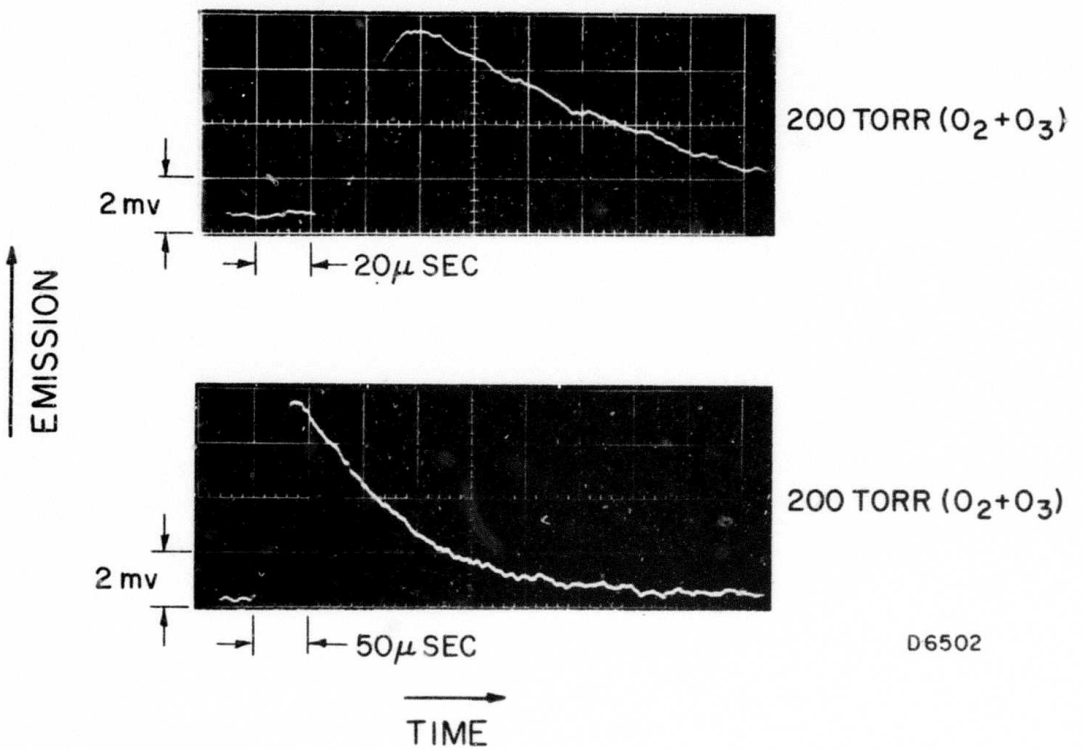

Figure 6 IR Emission from $O_3^{\dagger}$ Formed from Flashes in 0.31% O_3 + O_2 at 299 Torr. Two identical runs at different sweep rates are shown; ν_3-Band filter.

to peak signal. The characteristic time of the final decay scales with the square of the total pressure, as it should if the source of emission energy is from a recombination. If the source of emission is due to energy transfer to O_3 from a species formed in an excited state by the primary photolysis (e.g., $O(^1D)$ or $O_2(^1\Delta)$) or from any other reasonable mechanism we could conceive (involving subsequent cascade of the energy to make other excited species) then the time of this final decay would be controlled by a two-body process and would scale with the pressure rather than with the pressure squared as these results displayed.

2.4.2 $O_3 + O_2$ Kinetics

A summary of the kinetics we believe is occurring in these $O_2 + O_3$ runs is given in Figure 7. Here we plot room temperature characteristic times for the reactions of interest for our typical conditions. A primary photolysis of 32% is typical in our apparatus (our method for making this measurement will be described later).

A comparison of the various ozone absorption bands[7] with a curve showing the spectral output of our flashlamps, as supplied by the manufacturer, showed us that the strong region of the Hartley band ($\sim$2500 Å) must be responsible for our ozone photolysis; this means that[8-11]

$$O_3 + h\nu \rightarrow O(^1D) + O_2(^1\Delta) \qquad (7)$$

represents our photolysis. The $O(^1D)$ immediately quenches in collisions with O_2 to produce $O_2(^1\Sigma)$ and/or vibrationally excited O_2.[8-10] We use an efficiency of $^1\Sigma$ production of $\psi = 70\%$ which seems consistent with much of the data (summarized in Ref. 10). As will be seen the value of ψ is important to our data reduction. Figure 7 shows the competition for $O(^1D)$ by O_3 rather than O_2 loses by a factor of 100.[8,10] The $O_2(^1\Sigma)$ reacts with unphotolyzed O_3 to generate additional O-atoms in a time comparable to τ_d, the flashlamp discharge time.[8,10,17] Thus, our total O-atom production is the amount produced by primary photolysis multiplied by $(1 + \psi)$. The slightly delayed production of additional O-atoms by this mechanism may contribute to the somewhat sigmoid initial shape of the signal. The competing reaction for quenching of $O_2(^1\Sigma)$ by O_2 loses by over 100-fold.[18-21]

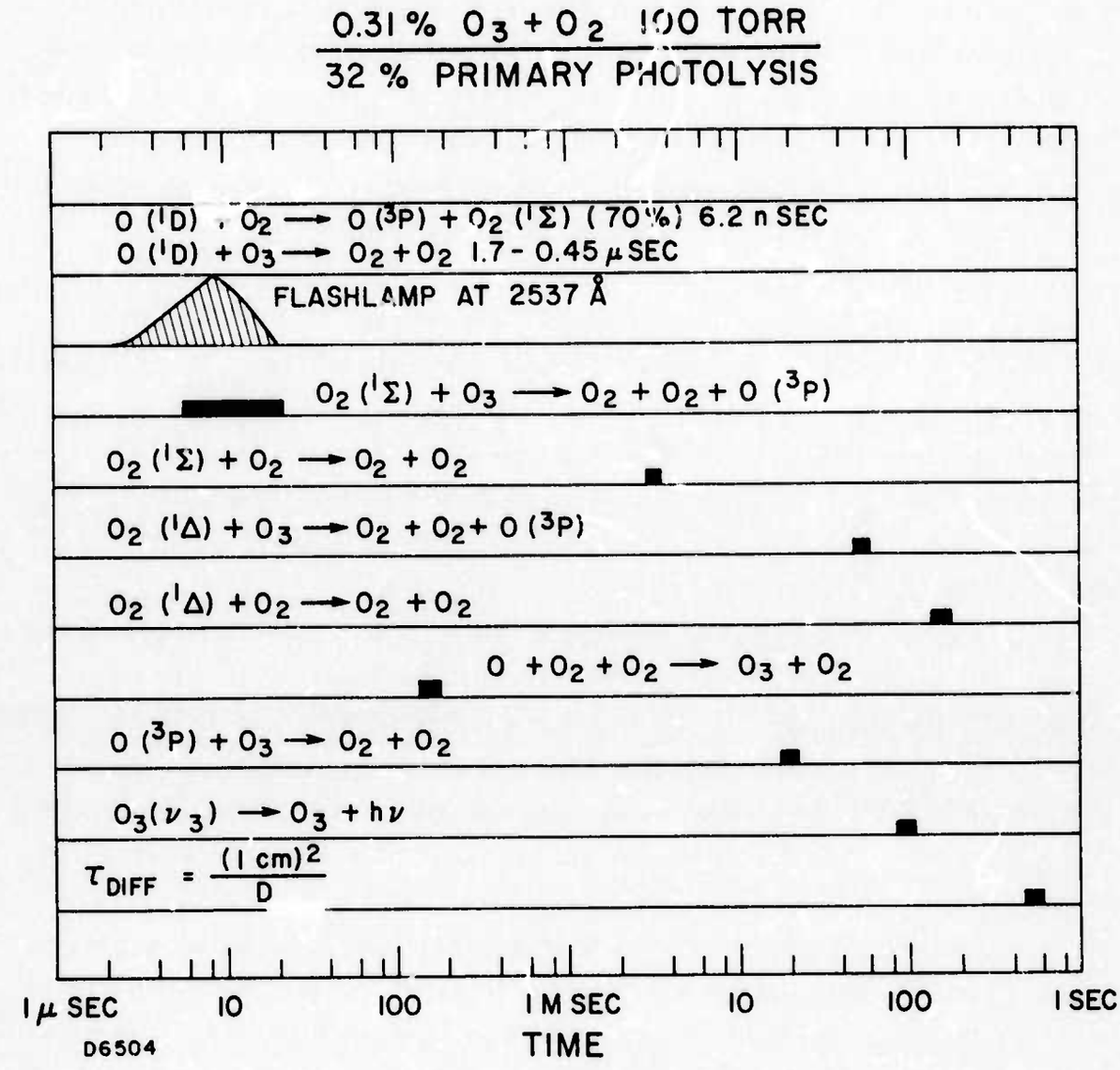

Figure 7 Display of Time Scale for Reactions of Interest for 0.3% O_3 + O_2 at 100 Torr with 32% Primary Photolysis

The quenching of $O_2(^1\Delta)$ by either O_2[22,23] or O_3[24-26] would seem to be very long compared to the recombination time, so that a small amount of $O_2(^1\Delta)$ persists throughout an experiment. Still, its concentration is only about 0.1% of the total O_2 so that it is only present in a small fraction of the recombinations. In fact, since it has 1 eV of excitation and the $O\text{-}O_2$ bond is 1 eV, one might expect $O + O_2(^1\Delta) + O_2 \rightarrow O_3 + O_2$ to be a rather improbable event even when the right collision partners are present. Further, the time scale of 50 msec for its quenching by O_3 rules it out as a direct source of excitation for the signals we observe.

Figure 7 shows the fate of ground state O-atoms is to recombine with O_2 to form ozone and not to react with ozone.[12-16,27]

Once formed vibrationally excited ozone is only lost through quenching reactions as radiative loss is negligible for our experiments since the radiative lifetimes are 2.82 sec, 4.03 sec, and 94 msec for the ν_1, ν_2, and ν_3 modes, respectively. Loss of reactants or excited products at any solid surface is denied by the long diffusion time at these pressures.

2.4.3 $O_3 + N_2$

We made a number of runs in 0.31% $O_3 + N_2$ (nominal) for two reasons. All of our theoretical understanding of the kinetics and the behavior of the signals from the $O_3 + O_2$ runs suggested that even if $O(^1D)$ quenching by O_2 or N_2 produced vibrational excitation that such an effect was not important in our study. Therefore we expected to see no IR emission from $O_3 + N_2$ runs. In fact, we did not see emission and this is illustrated by Figure 8.

The second reason for the $O_3 + N_2$ runs was to allow an experimental determination of the amount of primary photolysis of O_3 in our $O_3 + O_2$ runs. The kinetic basis for this is given in Figure 9. The principal differences between this figure and Figure 7 are: 1) the fast quenching of $O(^1D)$ by N_2[18,28-30] does not lead to additional O-atom production as the $O_2(^1\Sigma)$ sequence did; and 2) after the flash no significant kinetics occur for over 10 msec. Thus, by measuring $[O_3]$ before the flash and at t = 100-200 μsec, we have a measurement of the primary photolysis.

2.4.4 Recombination Rate k_1

The $O_2 + O_3$ data as shown in Figure 6 were first analyzed to obtain the characteristic time τ_f, of the final exponential decay. Several runs

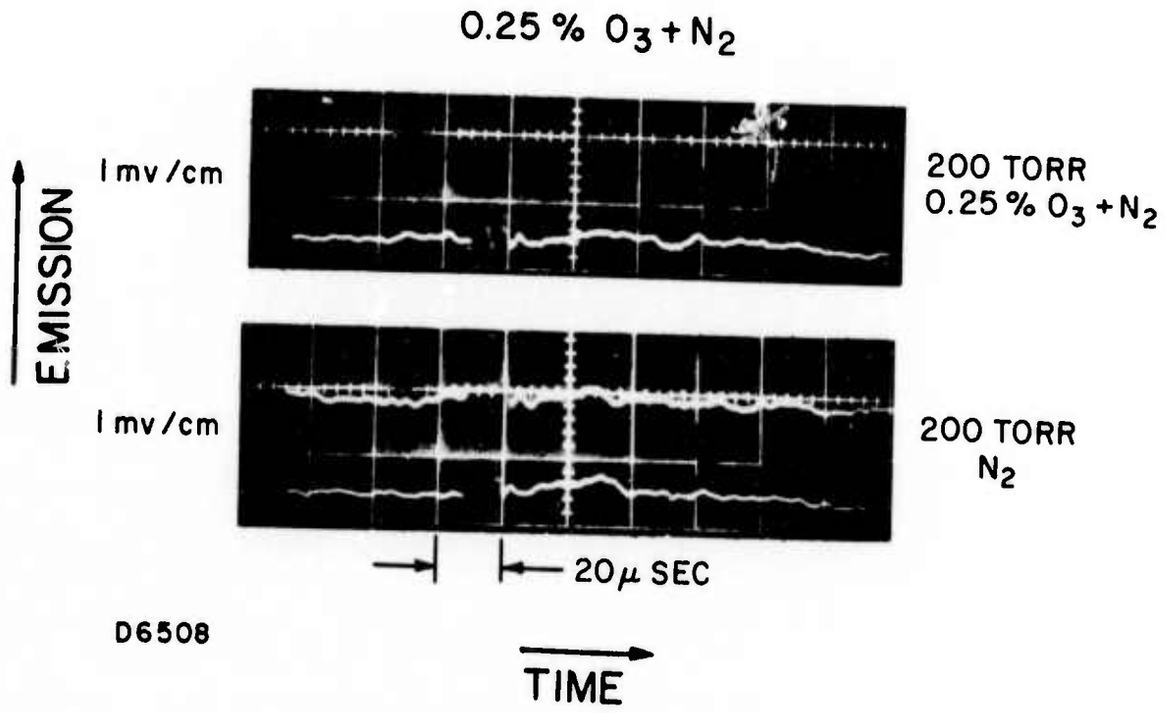

Figure 8 IR Detector Signals for Runs in 0.25% $O_3 + N_2$ and Pure N_2. As expected no emission is observed in either case; ν_3-Band filter.

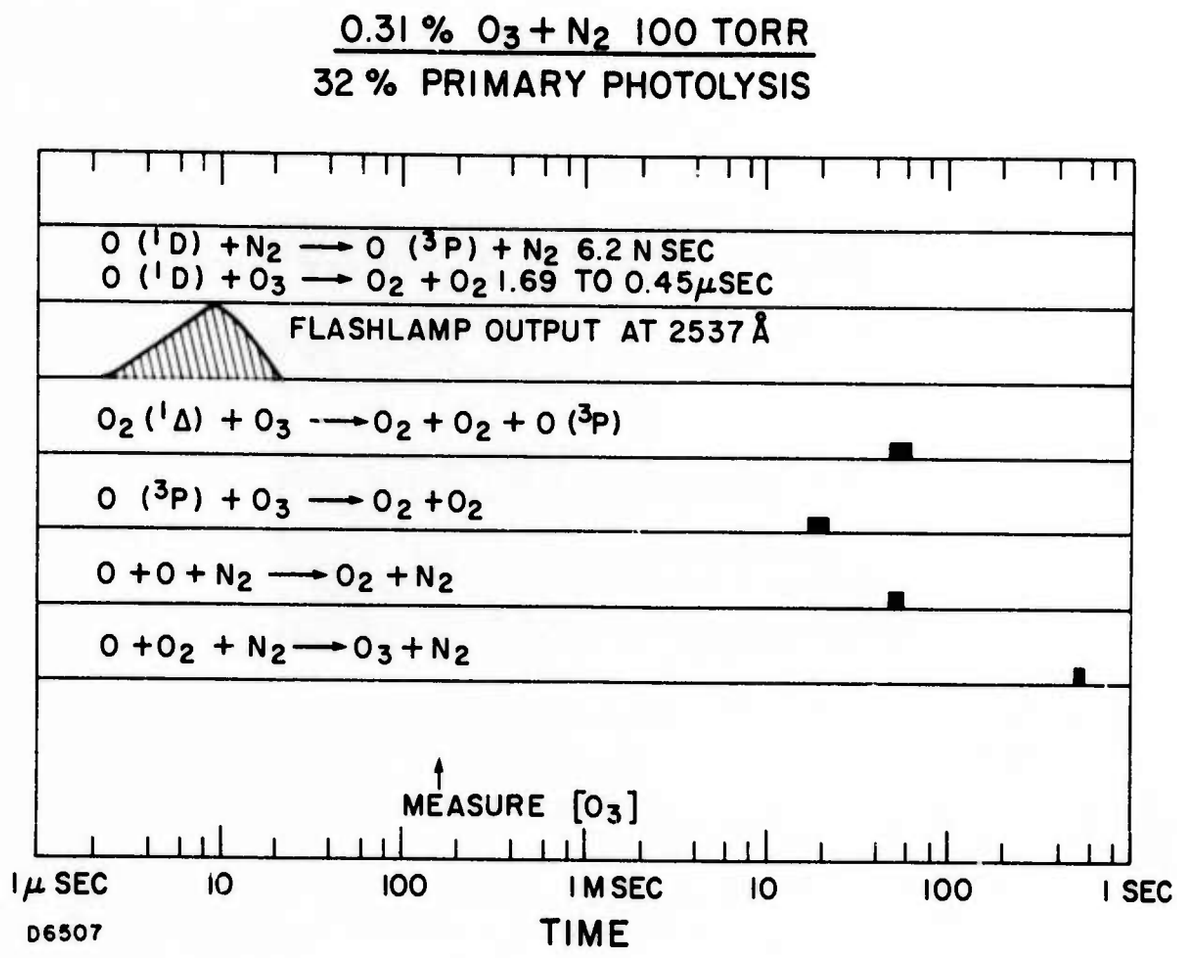

Figure 9 Display of Time Scales for the Reactions of Interest for 0.25% O_3 + N_2 at 100 Torr with 32% Primary Photolysis. Also shown is the time at which we measure O_3 to learn the amount of primary photolysis.

were plotted on semi-log paper (log signal vs time) to verify their exponential behavior. For the bulk of the oscillograms we read the time in the manner illustrated in Figure 10, i.e., $t = \tau_f$ when $S = S'$ where $S' = S_f (1 - 1/e)$. Figure 10 shows these times vs pressure in a log-log plot. A line through the data has slope two and demonstrates the scaling with pressure squared as is appropriate for a recombination process. This line, which corresponds to a rate of $k_1 = 3 \times 10^{-34}$ cm^6 sec^{-1}, summarizes our measurements of process (1). A value of $k_1 = 6 \times 10^{-34}$ more nearly summarizes the prevailing literature value for this rate;[11-15] a line representing this value for k_1 is included in Figure 10.

2.4.5 Variations in $[O_3]$ and ψ

In doing runs on $(O_3 + O_2)$ it was possible to provide an initial filling with the test gas and then execute many flashes with some loss from flash to flash of ozone as evidenced by both transferse UV-absorption measurements and by the magnitude of the IR signals. The amount of ozone lost was enhanced by working at lower pressures; at 400 torr the decrease in peak IR signal between the first and the second flash when separated in time by less than a minute was only 1% while at 100 torr it was 9%. In general ozone would disappear in our cell with a loss of 63% (1-1/e) in about 15 minutes. This was presumably by decomposition at surfaces and was enhanced during the time just after a flash when surfaces were heated by flashlamp light and/or from the gas.*

Another feature of this data was that τ_f, the final decay time, was unaffected by whether it was obtained from the first flash on a mixture or a subsequent flash. This is illustrated in Figure 10 where at 200 torr in a sequence of 6 flashes (with several minutes allowed between flashes in order to enhance the loss of O_3) there was an 18-fold decrease in $[O_3]$. There was no systematic variation in τ_f with $[O_3]$.

*Gas heating is estimated at about $\Delta T = 18^{\circ}K$ based on an energy deposition of [(0.3% ozone) * (30.% photolysis) * (2 eV for the $O(^1D)$ + 1 eV for the $O_2(^1\Delta)$ + 1 eV for the $O + O_2 \rightarrow O_3$ bond)] = 5/2 $k\Delta T$. The energy deposited due to the production of O by O_2 photolysis is small in comparison.

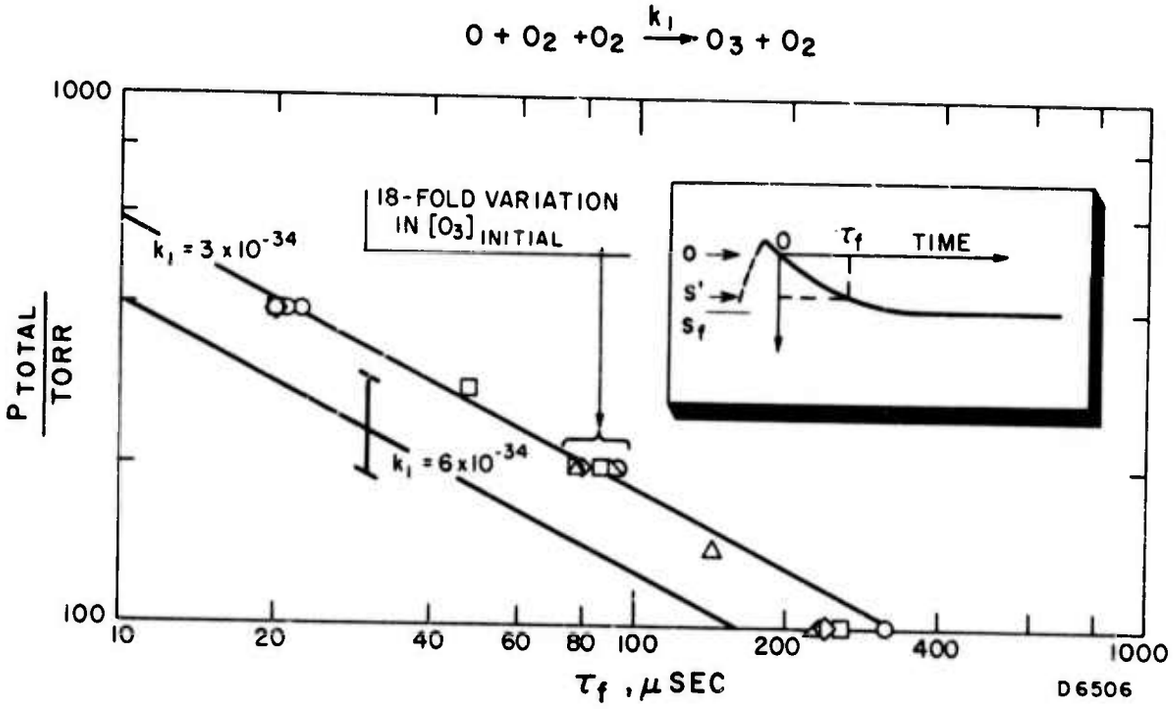

Figure 10 Characteristic Time of the Final Exponential Decay of the IR Signals vs Total Pressure. A pressure dependence of $\tau_f \propto p^2$ is indicated by the line fitting the data, which corresponds to an $O + O_2 + O_2 \rightarrow O_3 + O_2$ recombination rate of $k_1 = 3 \times 10^{-34}$ cm^6 sec^{-1}. The prevailing literature values of $k = 6 \times 10^{-34}$ are represented by the other line. All data are for mixtures of O_2 + 0.31% or less O_3. At 200 torr $[O_3]$ - initial varied by a factor of 18 with no systematic change in τ_f. All data for ν_3 - band filter.

2.4.6 Vibrational Relaxation

The time to peak signal, t_{max}, was determined for each of the $(O_3 + O_2)$ runs as illustrated by the sketch in Figure 11. This figure shows a plot of t_{max} vs ϕ as suggested by Eq. (6) with these results fitted by adjusting k_2 to the value 2×10^{-14} cm^3 sec^{-1} when $k_1 = 3 \times 10^{-34}$. As discussed this fit is strongly dependent on k_2 and only weakly on k_1, especially for the lower pressures where there is a good separation of the time scales $\tau_d < \tau_v < \tau_r$. As an approximate correction, the 3.25μsec detector response is added to Eq. (6) before plotting in Figure 11. A more important correction would be the temporal distribution of the flashlamp output. For visual comparison this is shown at the right of Figure 11. A proper accounting of this effect would presumably require an integration of the kinetic rate equations including a term for the production of O-atoms in time proportional to the flashlamp output at 1800 Å.

For further experimental verification of our model and the relation of t_{max} to $O_3^\dagger$ vibrational relaxation we decided to add water vapor to our O_3/O_2 mixes. We suspected H_2O should be efficient in vibrationally relaxing O_3 and its presence did indeed reduce the time to t_{max} by about two-fold when 1 torr of H_2O was added at 200 torr total pressure; data are shown in Figure 11 by the X's. This would suggest a relaxation of $O_3^\dagger$ by H_2O with a rate of about 4×10^{-12} cm^3 sec^{-1}, although our evidence for this value is limited.

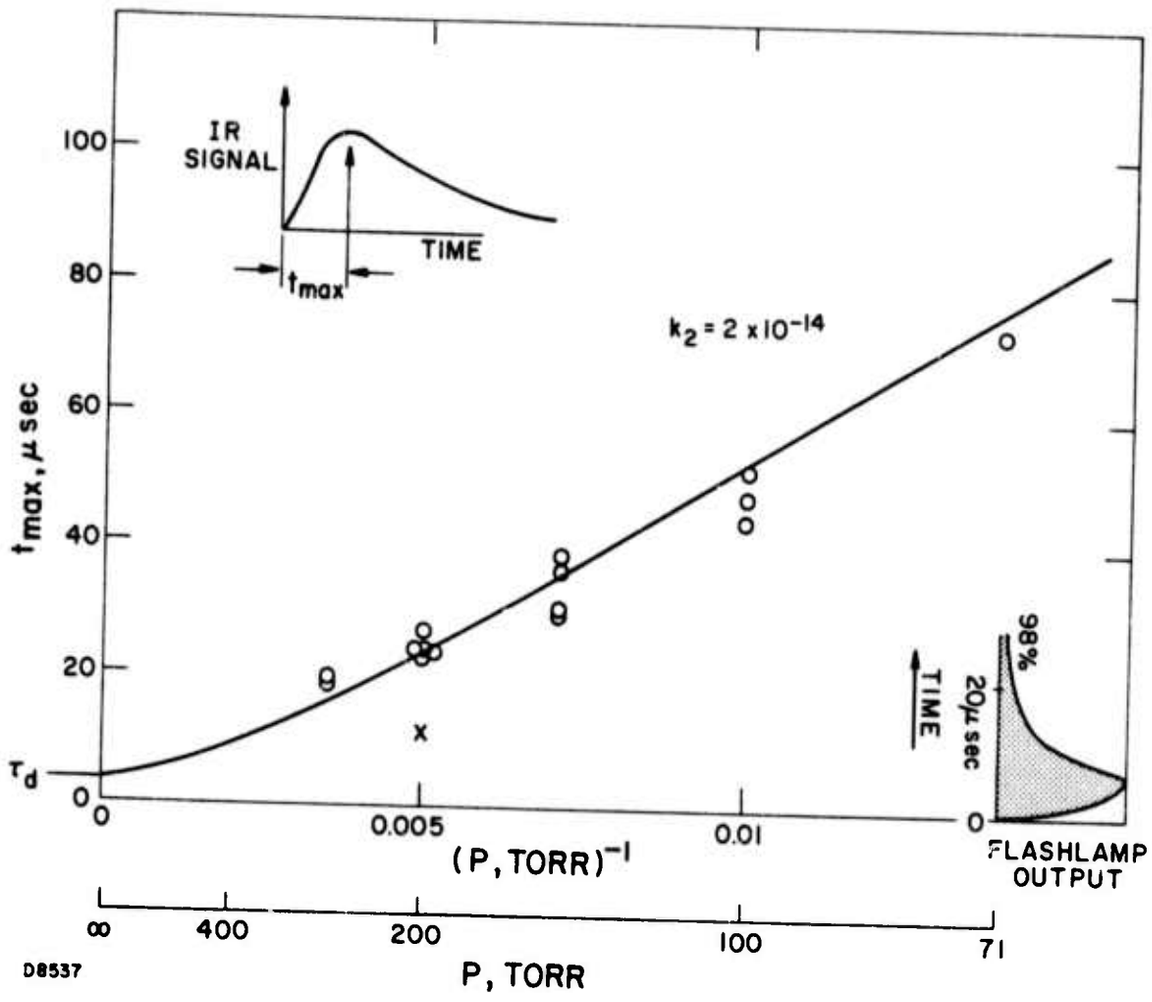

Figure 11 Time to Peak Signal t_{max} from the Start of the Signal Rise (Found by Extrapolating Backward in Time as Indicated in the Sketch) vs $1/p$; t_{max} relates to k_2, the rate of vibrational relaxation of O_3 (ν_3-band filter), and is fitted by the line which represents Eq. (6) for $k_2 = 2 \times 10^{-14}$ cm^3 sec^{-1}; O - 0.31% O_3 or Less + O_2, X - same mixture with 1 torr (0.5% at 200 torr) of H_2O added. A side plot of the flashlamp output (at 2537 Å) vs time is included.

2.4.7 Quantum Yield, ϕ

The reduction of our data by use of Eq. (5) evaluated at $t = t_{max}$ with the peak data signals read from oscillograms is described in Appendix A, which also describes the small corrections for self-absorption which were necessary in the ($O_2 + O_3$) data. The results are plotted in Figure 12 as

$$f = \frac{[O_3 (v = 1)]}{[O]_o}$$

and are compared to theoretical predictions using the simple two level model. There is no ambiguity in the pure O_2 data and they would seem to imply $\phi \simeq 0.6$ to 1.0. The reduction of the $O_3 + O_2$ data depend on the choice of ψ; our reduction assumed $\psi = 0.7$, for which there seems to be reasonable agreement between the two sets of data. A reasonable summary of our data would be that $\phi = 0.8$.

As discussed earlier the quantity ϕ has a great utility in presenting our experimental results in an unambiguous fashion. Its deeper meaning however depends on what in fact occurs in the recombination. For example if recombination is allowed into each level of the vibrational ladder of the mode of interest with a rate $\phi_v k_1$, i.e.,

$$O + O_2 + O_2 \xrightarrow{\phi_v k_1} O_3 (v) + O_2,$$

and V-V shuffling occurs in a time $\tau_{vv} < \tau_v$* in the presence of excess initial $O_3(v=0)$ then ϕ is replaced by $\Sigma\, v\phi_v$ in the steady state solution for the signal. Actually quite a number of assumptions about the nature of the recombination and vibrational relaxation are possible; some of the simpler cases are presented in Appendix B. One basic question raised by these models is the general relation of the time scales of the recombination, the V-V, and the V-T relaxation processes. This is important because if the V-V "shuffle" processes are slow compared to the recombination then one can say that the emission is due to an initial distribution controlled by the ϕ_v rather than representing a constrained (conservation of quanta) redistribution of the quanta by V-V shuffle. The important time

*where τ_v represents V-T deexcitation plus V-V transfer to other O_3 modes or to O_2.

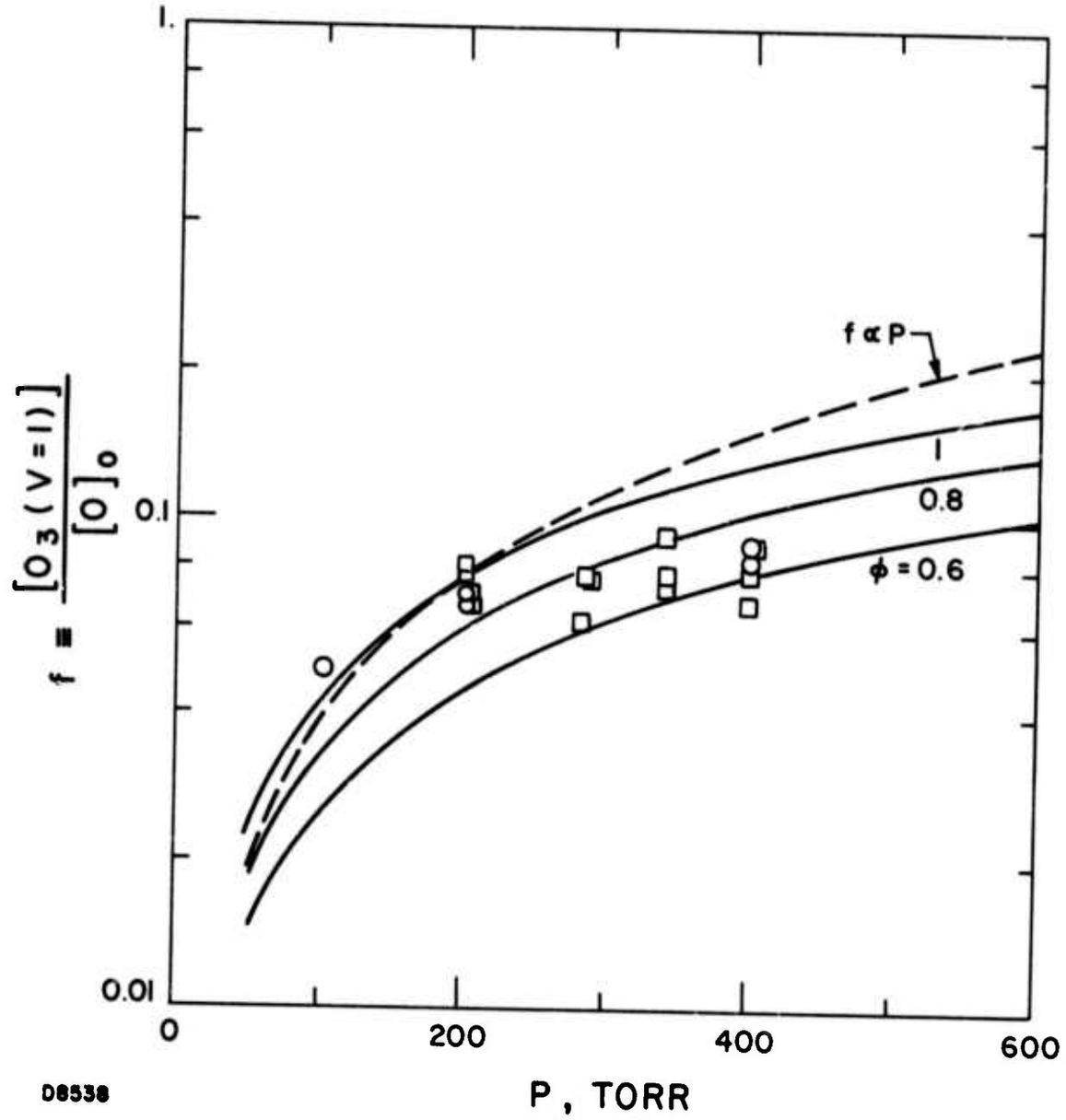

Figure 12 The quantity f vs pressure is derived from oscillograms of IR emission as explained in Appendix A, and compared to the theoretical curve representing Eq. (A-1) for various ϕ with $k_1 = 3 \times 10^{-34}$ and $k_2 = 2 \times 10^{-14}$, - Pure O_2 Runs, O; 0.31% $O_3 + O_2$ runs reduced with $\psi = 0.7$, □. Dashed line, which scales f linearly with pressure, shows that Eq. (A-1) has approximately that dependence.

scales are compared in Figure 13. On this log-log plot the recombination has slope two, while the relaxation processes have slope unity. Because of this, their relationship changes with pressure and interesting changes occur where lines intersect. It is apparent, as we discussed in Section 2.3, that at the pressures of our work $\tau_{vt} < \tau_r$ is true. The relation between τ_{vv} and τ_r depends on the mole fraction of ozone. We have somewhat arbitrarily chosen the V-V rate constant indicated (1×10^{-11}) in order to make this figure. The process

$$O_3(v) + O_3(v') \rightarrow O_3(v-1) + O_3(v'+1) \tag{8}$$

no doubt depends strongly on $|v - v'|$; e.g., if in the initial stages $v' = 6$ is largely formed and the background (unphotodissociated) O_3 is in $v = 0$, then, due to the anharmonicity of the ozone potential, process (8) would be much less probable than if $v' = 6$, $v = 6$. By the time intramolecular processes are included the whole business gets quite complicated with far more unknowns than observable features on the data or the number parameters which we can vary to separate various effects. A summary would say that processes of type (8) are improbable in the pure O_2 data but probable in the (0.3% O_3 + O_2) data for times of order of the recombination time. The processes

$$O_3(v) + O_2 \rightarrow O_3(v-1) + O_2 \tag{9a}$$

or

$$\rightarrow O_3(v-1) + O_2^{\dagger} \tag{9b}$$

are "measured" by our k_2 whether or not Reaction (9a) results in transfer to another ozone mode. Since our value of ϕ obtained from the pure O_2 data is comparable to that from the $O_3 + O_2$ data, it would seem that V-V

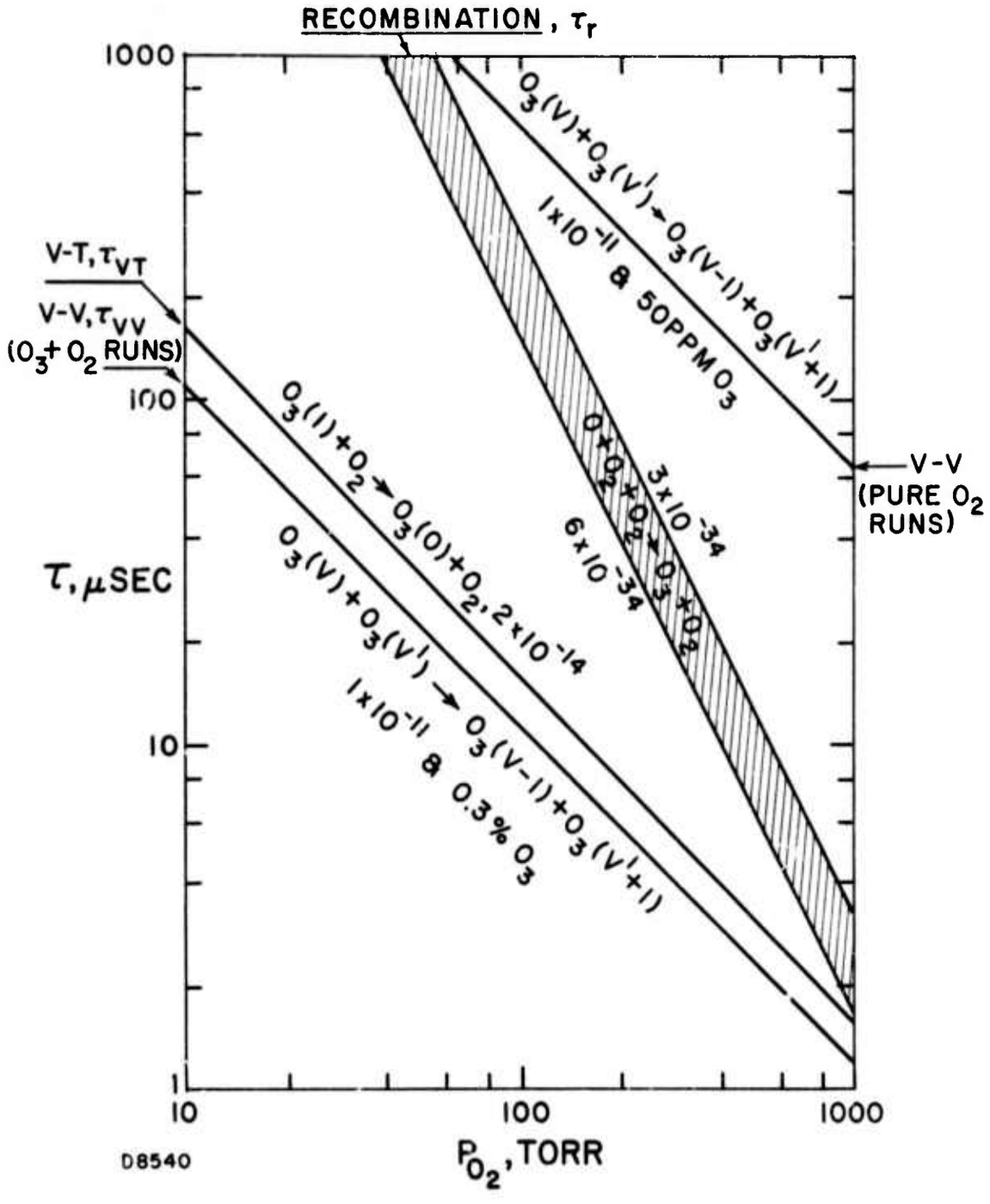

Figure 13 Characteristic Times for Various Kinetic Processes vs P_{O_2} for the Rates and Concentrations Listed. The recombination time τ_r, V-T time τ_{VT} and V-V times τ_{VV} are compared.

shuffling was not an important feature in our results. This coupled with experimental evidence, presented later, that upper levels of $O_3(\nu_3)$ are indeed populated suggests that only models for which ϕ, or its replacement in the particular models (e.g., $\Sigma v\phi_v$), is insensitive to V-V shuffle are correct. For example, (see Appendix B) models B-II, B-III or B-V, but not B-IV, are compatible.

2.4.8 Effect of N_2

It was desired to briefly investigate the effect of N_2 in this work as a collision partner for both the process

$$O + O_2 + N_2 \xrightarrow{\phi_N k_{10}} O_3(v=1) + N_2 \qquad (10)$$

and

$$O_3(1) + N_2 \xrightarrow{k_{11}} O_3(0) + N_2 \qquad (11)$$

In this work a mixture of 0.3% $O_3 + O_2$ was mixed with an equal part (by partial pressure) of N_2; the results are shown in Figure 14. Consideration of these oscillograms shows that for equal ozone concentrations in the initial mix (obtained by running the second mix at double the pressure of the $(O_3 + O_2)$ mix) one obtains an equal peak signal. This is consistent with an interpretation that has

$$\frac{\phi_N k_{10}}{k_{11}} = \frac{\phi k_1}{k_2}. \qquad (12)$$

Equation (12) says that N_2 is probably about the same as O_2 as a collision partner in both the recombination and the relaxation processes, but that if different then it is different in equal proportion for both processes. As a check on the latter possibility the three characteristic features (t_{max}, τ_f and S_{max}) were examined, and it seems that $k_{10} \simeq k_1$, which is consistent with others, k_{11} is slightly smaller than k_2 (by a factor of about 1.3), and therefore ϕ_N is also slightly smaller (by the same factor).

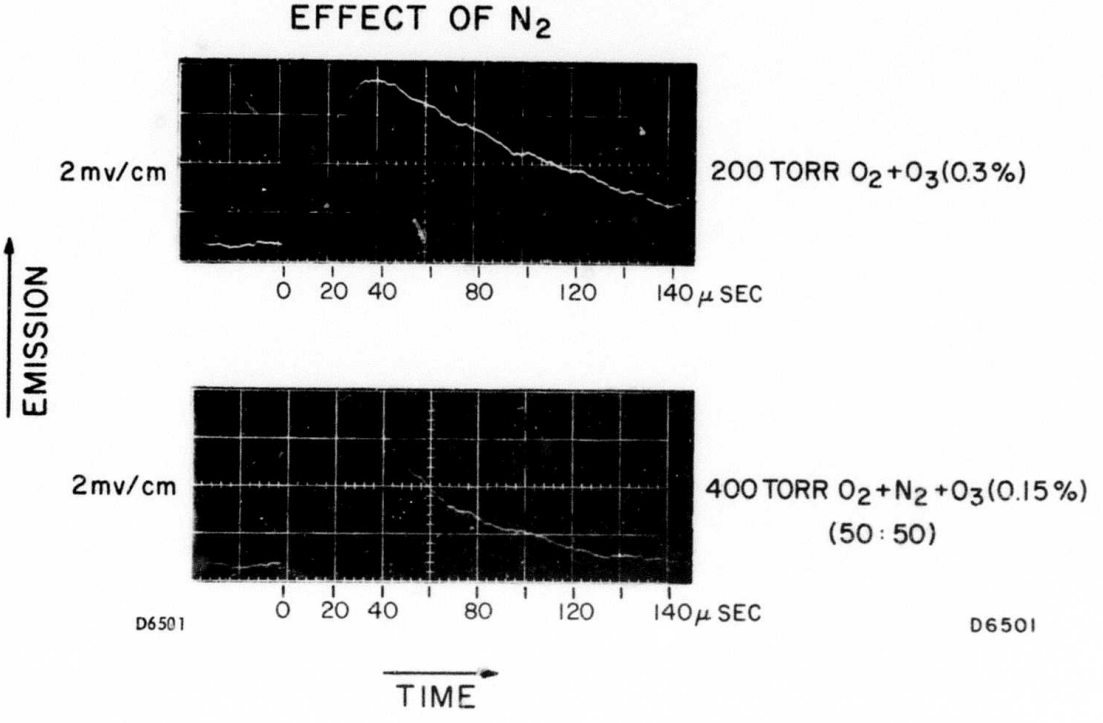

Figure 14 The effect of N_2 on the IR emission (ν_3-band filter) is illustrated by these two oscillograms.

2.4.9 "ν_3 - Upper Levels" Filter

One question of interest is whether the higher vibrational levels of a particular mode are populated in the recombination process. Figure 2 shows the "upper levels" filter we used to address this question for the ν_3-mode. This filter transmits in a region where there is very little absorption by room temperature ozone, and therefore presumably negligible emission from $\nu_3 = 1 \rightarrow 0$ transitions of ozone with a room temperature rotational temperature. Figure 15(b) shows an oscillogram resulting from such a run. These signals seemed to have essentially the same temporal characteristics as the "ν_3-filter" runs; i.e., for the run shown $\tau_f \simeq 75\mu$sec and $t_{max} = 23\mu$sec which place them in Figures 10 and 11 with the same values as the "ν_3-filter" data. The signal at the peak is less by about three-fold. Quantitative reduction of this signal level requires an assumption about what radiative lifetime is appropriate for the ν_3-levels that are principally responsible for the emission. For example, if $\nu_3 = 3 \rightarrow 2$ is the main contribution to the signal and $\tau_v = \tau_1/v$, as is appropriate for a harmonic oscillator,[31] then $\tau_3 = \tau_1/3$ and the peak signal in Figure 15(b) corresponds to an $[O_3(v=3)]$ that is 12-fold lower than the $[O_3(v=1)]$ obtained from the reduction of the Figure 15(a) peak signal. The appropriateness of these assumptions or of any simplified analysis of the data is difficult to evaluate since very little is known about the potential function for these normal modes, nor is anything known about the radiative lifetimes or collisional quenching rates of higher levels. If one adopts the potential model and constants of McCaa and Shaw[6] the vibrational levels of ν_3 would be located as shown in Figure 2. It is clear that the width of the band due to rotational struction ($\Delta\omega_r$ = width of ν_3 band in Figure 2 $\simeq 920$ cm^{-1}) is large compared to the energy decrease between levels due to anharmonicity ($\Delta\omega_v \sim 30$ cm^{-1}) and that to interpret even spectra with resolution better than $\Delta\omega_v$ would be a formidable task.

It is appropriate to note that Figure 15(b) does clearly show emission from upper levels since the signal is only down by three-fold from "ν_3-filter" data while the convolution of the ν_3-band with the "upper levels" filter is much more than three-fold different than its convolution with the "ν_3-filter," i.e., Figure 15(b) is not just $\nu_3 = 1 \rightarrow 0$ transitions coming through the wing of the "upper levels" filter.

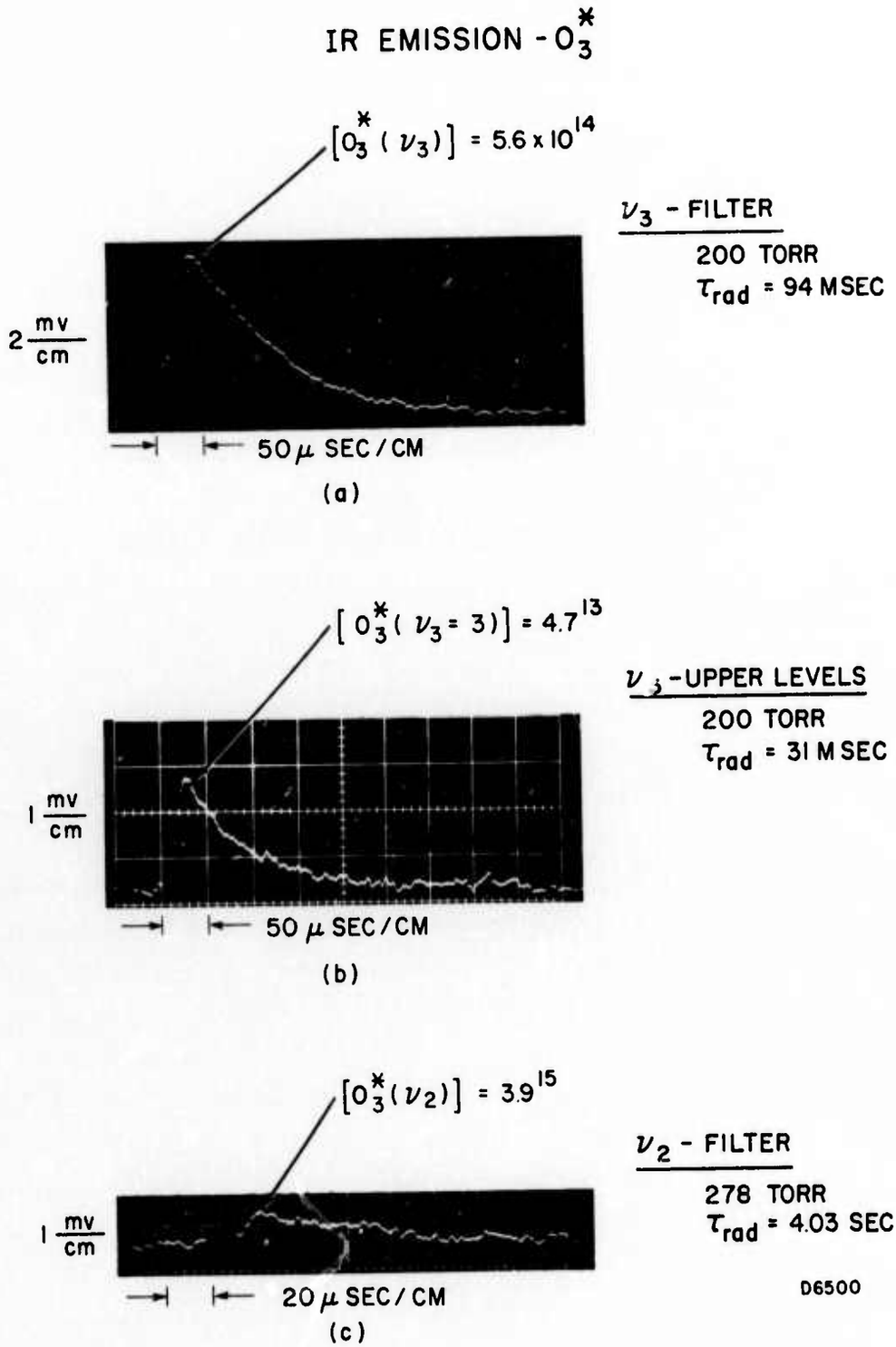

Figure 15 Comparison of Oscillograms Showing IR Emissions with Each of the Three Filters Illustrated in Figure 2.

Given this conclusion it is appropriate to question whether upper level population occurs directly in the recombination or by V-V shuffle. For example, if one has every O_3 formed in v = 1, with no excess O_3 then V-V shuffle without loss of quanta, in a harmonic oscillator approximation, generates a distribution represented by a vibrational temperature of 2160°K for the O_3 ν_3-mode. If there are two O_3(v = 0) for every O_3(v = 1) formed (as is the case in these experiments) then a distribution characterized by T_v = 1080°K would occur from V-V shuffle with no loss of quanta. If there is unlimited excess O_3 in v = 0 one tends to T_v = 0°K in this model, but of course the reality is that $T_v \rightarrow$ room temperature as the excess initial ozone dominates the conditions. The manner in which these numbers are obtained is indicated in Appendix C. The conditions most closely approximating our work are for 32% photolysis of the initial O_2 and 0.8 quanta formed per recombination implying N/Q = 2, 3 where N = total no. O_3 and Q = ns. quanta.* This gives a T_v = 1250°K after V - V shuffle.

We next desired to compare the radiation signals expected for the two system configurations (ν_3-band and ν_3-upper levels) for T_v = 1250°K with T_r = 300°K. This was done by first generating synthetic ozone spectra in the manner indicated in Appendix D. The spectrum for T_v = 1250°K and T_r = 300°K, was then multiplied by the relative spectral responses of the two detector/filter configurations and integrated over wavelength to obtain

$$\frac{S_{\nu_3}\text{-band}}{S_{\nu_3}\text{-upper levels}} = 18.$$

Since this is much larger then the ratio of 3, found from the data we conclude that ozone is formed preferentially in higher vibrational levels of ν_3 in the recombination.

One assumption here has been the neglect of V-T deexcitation; since these rates normally increase with increasing V-level the effect is to make

* $(0.32 \times (1 + \psi) \times 0.8)^{-1}$, $\psi = 0.7$

the above conclusion even more justified. Other uncertainties include the possibility of effects due to anharmonicity which would lead to a non-Boltzmann distribution in the vibrational levels[32, 33] and the possibility of energy transfer from the ν_2-mode by fast intra-molecular V-V shuffle.

2.4.10 $\underline{\nu_1}$-Mode

The most reasonable conclusion about the state of the ν_1-mode in this work is that it is in V-V equilibrium with the ν_3-mode. If

$$O_3(\nu_3) + O_2 \rightarrow O_3(\nu_1) + O_2$$

has a rate of $k \geq 1 \times 10^{-14}$ cm^3 sec^{-1}, which is almost assuredly true, then this process will be 10μsec or faster at all pressures used in this study. This means that in fact all of our ν_3-mode observations could be due to recombination giving vibrational excitation in the ν_1-mode which then transfers to the ν_3-mode; or the reverse could be true. In any case; if they are in V-V equilibrium and $\phi = 0.8$ has been deduced for the ν_3-mode in the manner outlined thus far, then one should deduce $\phi = 0.8$ for the ν_1-mode also and recognize that in fact any combination that satisfies $\phi(\nu_1) + \phi(\nu_3) = 1.6$ is a possible explanation for our data.

2.4.11 $\underline{\nu_2}$-Mode

The signals from the ν_2-mode, as evidenced by Figure 15(c), had fairly low signal-to-noise due to the long (4.03 sec) radiative lifetime of this mode. For 7 runs at 278 torr we read t_{max} and peak signals and applied the same analysis as was applied to the ν_3-data. It was not useful to deduce a k_1 from the final decay since this is known from the other data and the ν_2 signals are of low S/N; from Figure 15, however, it is clear that the final decay time is reasonable. The results of the analysis were $k_2(\nu_2) = 2.3 \times 10^{-14}$ and $\phi(\nu_3) = 3.7$. For this data reduction the value of

$$\int D_\lambda f_\lambda \, d\lambda$$

(see Appendix A), where D_λ is the detection system spectral response and f_λ is the spectral emission function of the radiating band, is somewhat more

critical than in our ν_3-band data reduction. This is because the filter does not cover the entire band (see Figure 2) and of course the exact nature of the spectral response function f_λ is not known for the conditions of non-equilibrium population peculiar to this experiment. It is reasonable, however, to presume that the shape of the absorption function shown in Figure 2 is mainly controlled by rotational structure with $T_r \simeq 300^\circ K$; population of higher vibrational levels would presumably show changes in band shape analogous to those illustrated in Figure 16 for the ν_3-band. For the reduction we simply used the emission band shape for this band with $T_v = T_r = 300^\circ K$.

2.4.12 Total Energy

If we use $\phi(\nu_1) = \phi(\nu_3) = 0.8$ and $\phi(\nu_2) = 3.7$ then this accounts for 50% of the exothermicity of the recombination process. One hazard in this conclusion is that the energy in the ν_2-mode may in part have come through the ν_3/ν_1 modes and therefore be counted twice (which would make the 50% an upper bound). The 50% could be presumed low if one considers that excitation of higher ν_2-levels is important and that much of the radiation from that band was missed due to this effect.

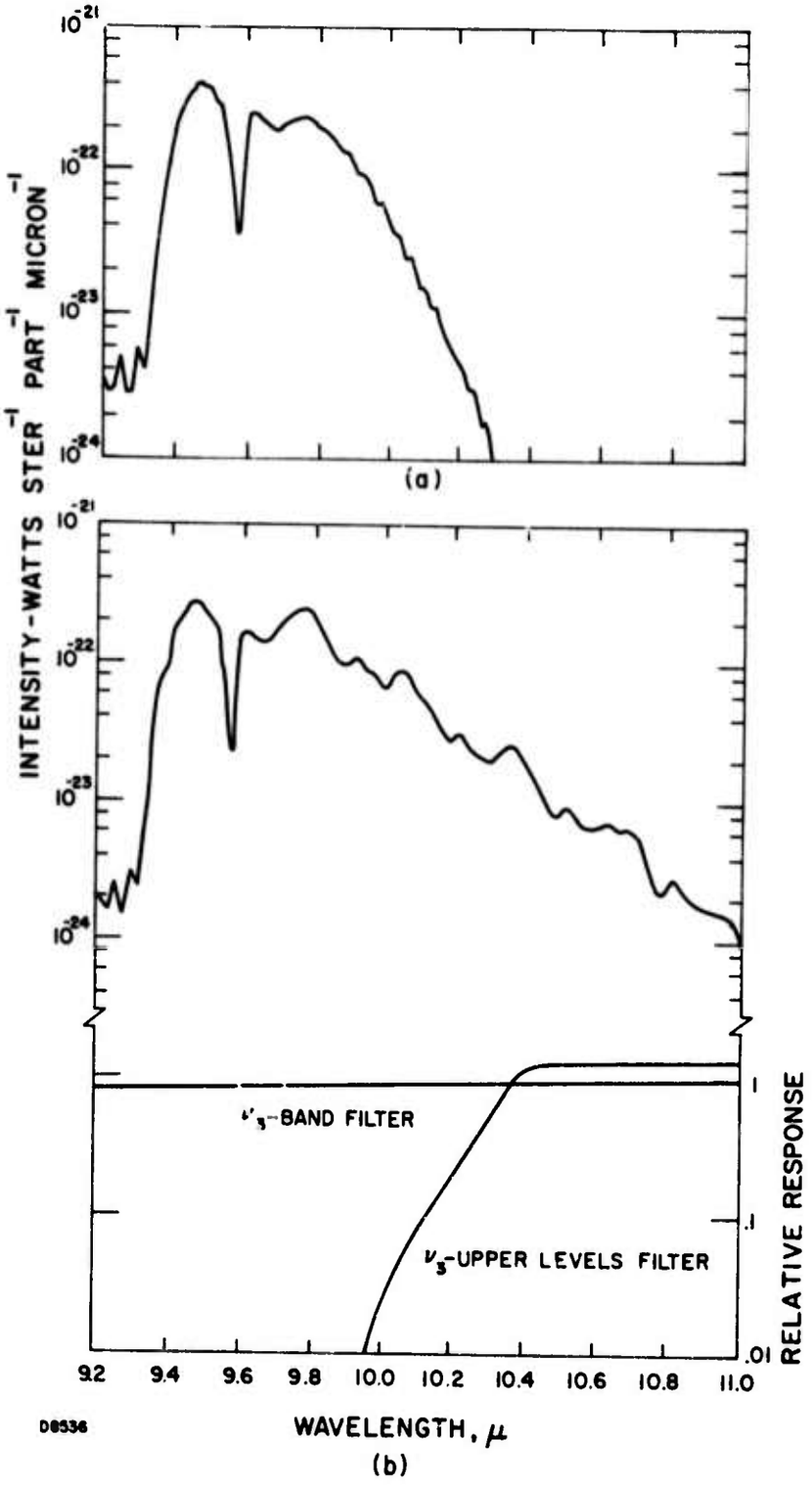

Figure 16 Synthetic Spectra for Ozone Emission: (a) for $T_v = 300^oK$ and $T_r = 300^oK$, (b) for $T_v = 1250^oK$ and $T_r = 300^oK$

3.0 CO_2/O_3 LASER ABSORPTION STUDIES

C. W. von Rosenberg, Jr. and Andrew Lowenstein

3.1 INTRODUCTION

To study kinetic processes involving vibrationally excited ozone it is necessary to know the rate for collisional deactivation of excited ozone. The laser fluorescence technique has proved very useful in studying similar relaxation phenomena.[34-36] The technique relies upon a resonant or near-resonant exchange of energy between a laser radiation field and an atomic or molecular system. The energy exchange excites the atomic or molecular system to a nonequilibrium state. If appropriate diagnostics are available, the relaxation of the system can be followed.

To study ozone vibrational relaxation a CO_2 laser was proposed as a source of excitation. Figure 17 shows the possibility of the 001-020 CO_2 laser transition exciting the first and/or third vibrational modes of ozone. The degree of excitation that can be achieved will depend upon the relative positions of the CO_2 and ozone spectral lines and whether a coincidental overlap occurs. The widespread interest in CO_2 lasers had led to a very accurate determination of the CO_2 rotational spectra[37] or laser line positions. Unfortunately, the difficulties of handling ozone and the complexity of its rotational spectra have resulted in far less information on the ozone spectra; most of the data has come from atmospheric studies.[38-42]

Because of the inadequate knowledge of the ozone spectra, an experimental study of the absorption of CO_2 laser radiation by ozone was first conducted. Absorption by ozone of several CO_2 rotational lines seemed quite likely, because of the high density of the ozone rotational spectra. The densities of the CO_2 and ozone rotational spectra are compared in Figure 18. Also shown are the approximate linewidths for the laser radiation, determined by cavity losses, and a Doppler broadened ozone rotational line. It is noted that the probability for overlap of the CO_2 and ozone spectral lines can be increased by collisionally broadening the ozone lines.

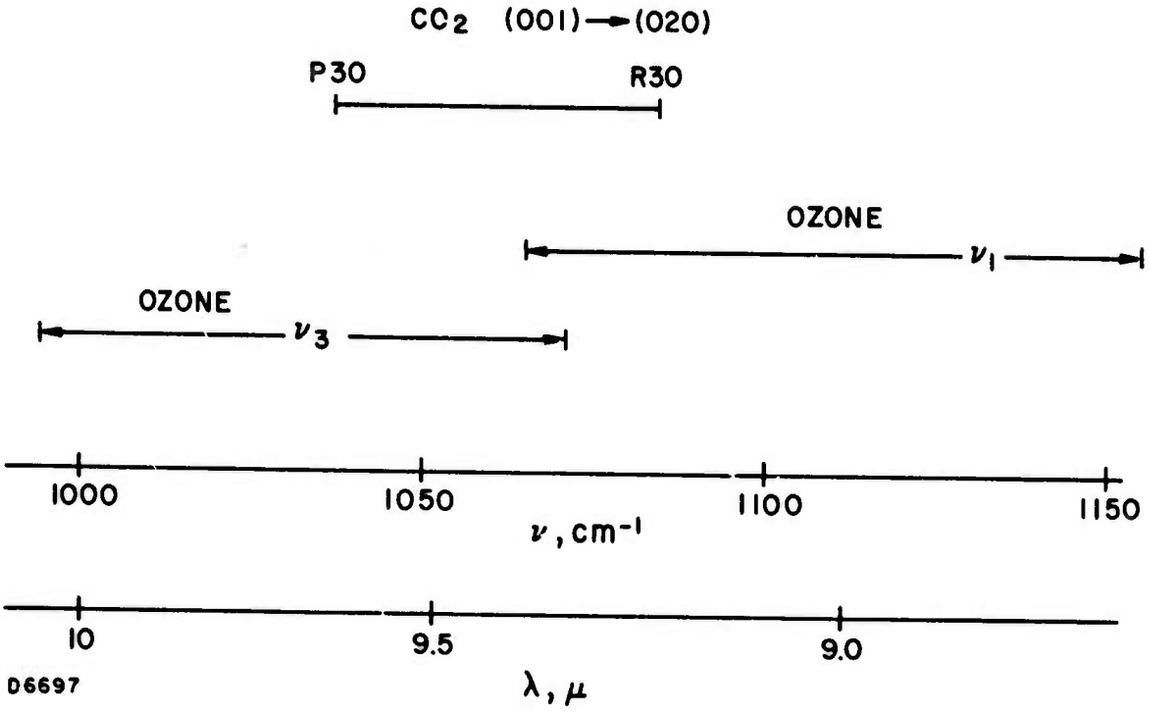

Figure 17 Spectral Overlap of the 9.6μ CO_2 Laser Lines with the Ozone Bands.

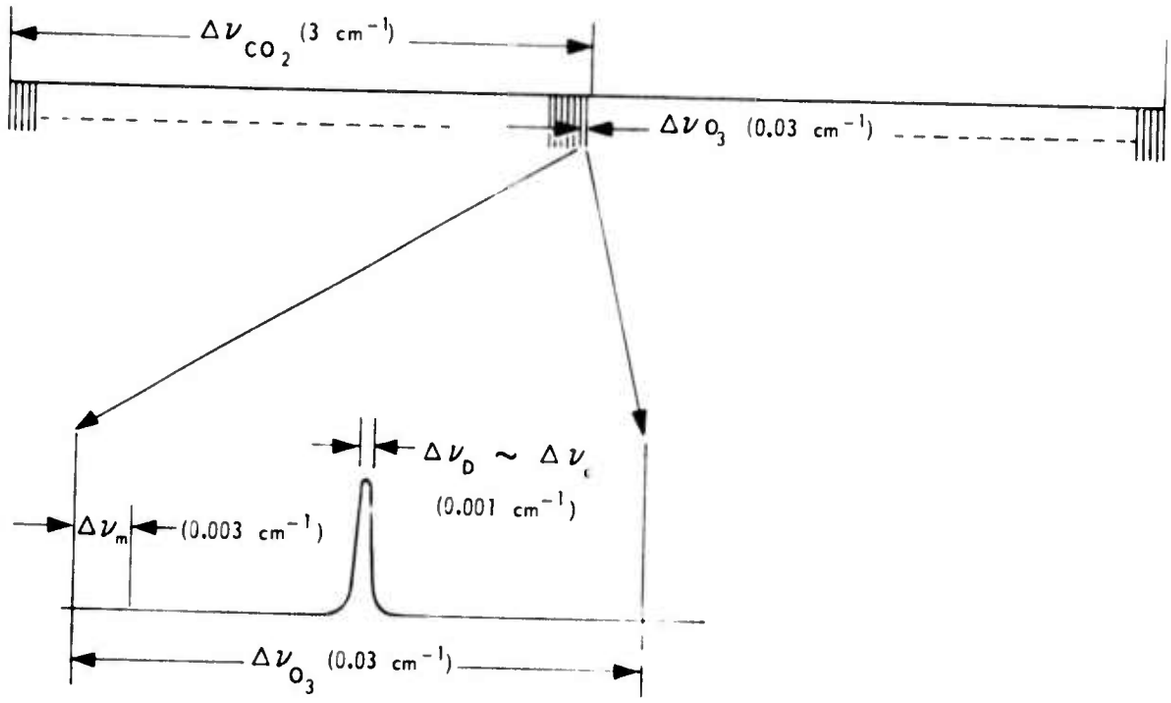

I $\Delta\nu_{CO_2}$ - SEPARATION OF CO_2 ROTATIONAL LINES $\sim$ 3 cm^{-1}

II $\Delta\nu_{O_3}$ - SEPARATION OF OZONE ROTATIONAL LINES $\sim$ 0.03 cm^{-1}

III $\Delta\nu_m$ - SEPARATION OF LASER CAVITY MODES $\sim$ 0.003 cm^{-1}

IV $\Delta\nu_D$ - DOPPLER LINE WIDTH $\sim$ 0.001 cm^{-1}

V $\Delta\nu_c$ - LINE WIDTH OF LASER RADIATION. FOR HIGH LOSS CAVITY THE LINE WIDTH WILL BE LIMITED BY WIDTH OF GAIN PROFILE. $\Delta\nu_c \sim 0.001$ cm^{-1}

D6699

Figure 18 Spectral Density of Ozone and CO_2 Lines in the 9.6μ Region, and Associated Line Widths.

A secondary objective of this study is the determination of the rate constant for the vibrational relaxation of CO_2 by ozone. This objective is a direct extension to ozone of the CO_2 vibrational relaxation studies of Moore, et al.[35] It can be accomplished with a minor alteration to the ozone absorption apparatus.

3.2 ABSORPTION OF 9.6μ LASER RADIATION BY OZONE

3.2.1 Experimental Apparatus

Figure 19 depicts the apparatus used to measure the absorption of CO_2 laser radiation by ozone. The CO_2 laser was operated CW with a mixture of He, CO_2 and N_2 in the ratio 3:1:1 flowing through the 1 m discharge cavity. The laser operated at a total pressure of 10 torr by using a mechanical pump with a buffering volume. Concentric counter flow cooling water was used over most of the discharge length. The discharge was operated at 6 kV and 30 mA. The optical cavity was bounded by a diffraction grating and a mirror, both external to the discharge volume. The grating was from Baush & Lomb, 75 groove/mm, blazed for 10μ and operated in the first order. The laser was tuned to a particular rotational transition of CO_2 by adjusting the pitch of the grating. Single line operation was facilitated by use of an adjustable iris in front of the grating. The mirror was concave (4 m radius) and non-transmitting except for a 2.5 mm diameter hole for coupling energy from the cavity. Laser power output was approximately 0.7 watts as measured by a power meter.

A chopping disk was fitted with 1/2 inch copper mirrors in two of its four holes. When rotated, the disk alternately passed the laser beam through the absorption cell to an IR detector, and reflected the beam to a second IR detector.

The absorption cell was 22.8 cm in length, 2.54 cm in diameter with BaF_2 windows set at the Brewster angle. The cell was designed with a side arm that allowed the ozone concentration to be measured by the absorption of 2537 Å radiation with a penlight mercury lamp/photomultiplier (1P28) combination.

When tuning the laser to a particular line, the wavelength of the beam was monitored by a 1/4 meter Jarrell-Ash monochromator utilizing a 10μ

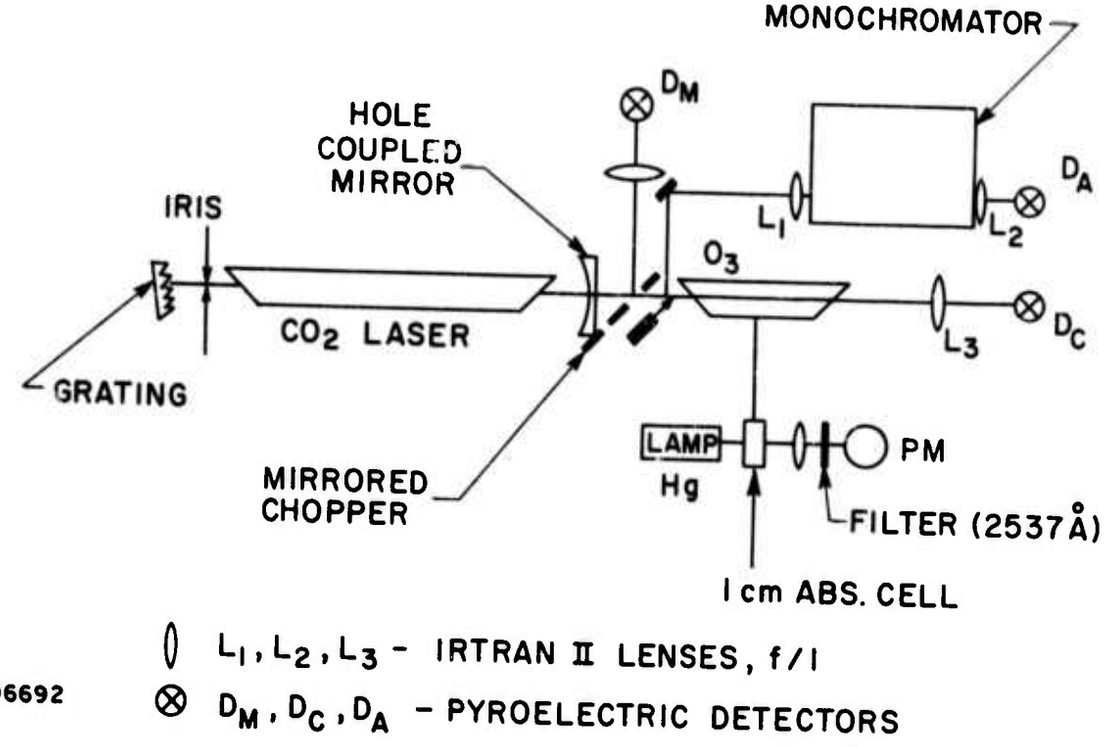

Figure 19 Experimental Apparatus for Measurement of Absorption by Ozone of CO_2 Laser Lines.

blazed, 50 grooves/mm grating. An IR detector was installed at the exit slit of the monochromator. All three IR detectors were T-301 pyroelectric detectors from Barnes Engineering.

3.2.2 Calibration

It was necessary to calibrate the monochromator for operation with the 10μ blaze grating. The higher order diffractions of 6328 Å radiation from a He-Ne laser, and 2537 Å radiation from a mercury lamp were used for the calibration. Figure 20 shows the expected linear relation between wavelength and monochromator reading.

With the test cell removed from the cavity, lasing could be sustained on all allowable 001 → 020 transitions within the range R32 → P46. Previously obtained values for the wavelength of these transitions[37] are also plotted versus monochromator reading in Figure 20.

The absorption measurements required determining the ratio I/I_o where I_o and I are the intensity of the beam before and after passing through the ozone sample. During an absorption measurement, the value of I_o was inferred from the intensity of beam reflected from the mirrored chopper. This required correlating the responses of the detector, D_M, which monitored the reflected beam, and the detector, D_C, which monitored the beam after passing through the cell. With the absorption cell empty the signals S_M and S_{C_o}, from the detectors D_M and D_C, respectively, were recorded for several different laser outputs. Figure 21 shows that S_M and S_{C_o} are linearly related and this relation is independent of the wave length or power of the laser radiation for the range of signals covered.

Absorption measurements were performed on several CaF_2 windows as a global check on the operation of the system. The test cell was removed, and polished CaF_2 windows of varying thickness were placed in the path of the beam. With the mirrored chopper revolving at 3900 rpm, the signals S_M and S_C were recorded on a single oscillograph (Figure 22(a)). Before and after each measurement, the wavelength of the laser radiation was checked with the monochromator. The unabsorbed signal S_{C_o}, was determined from its relation to the signal S_M as previously described. Because the pyroelectric detectors were operated in a linear range, the ratio S_C/S_{C_o} equaled the transmittance, I/I_o, of the sample.

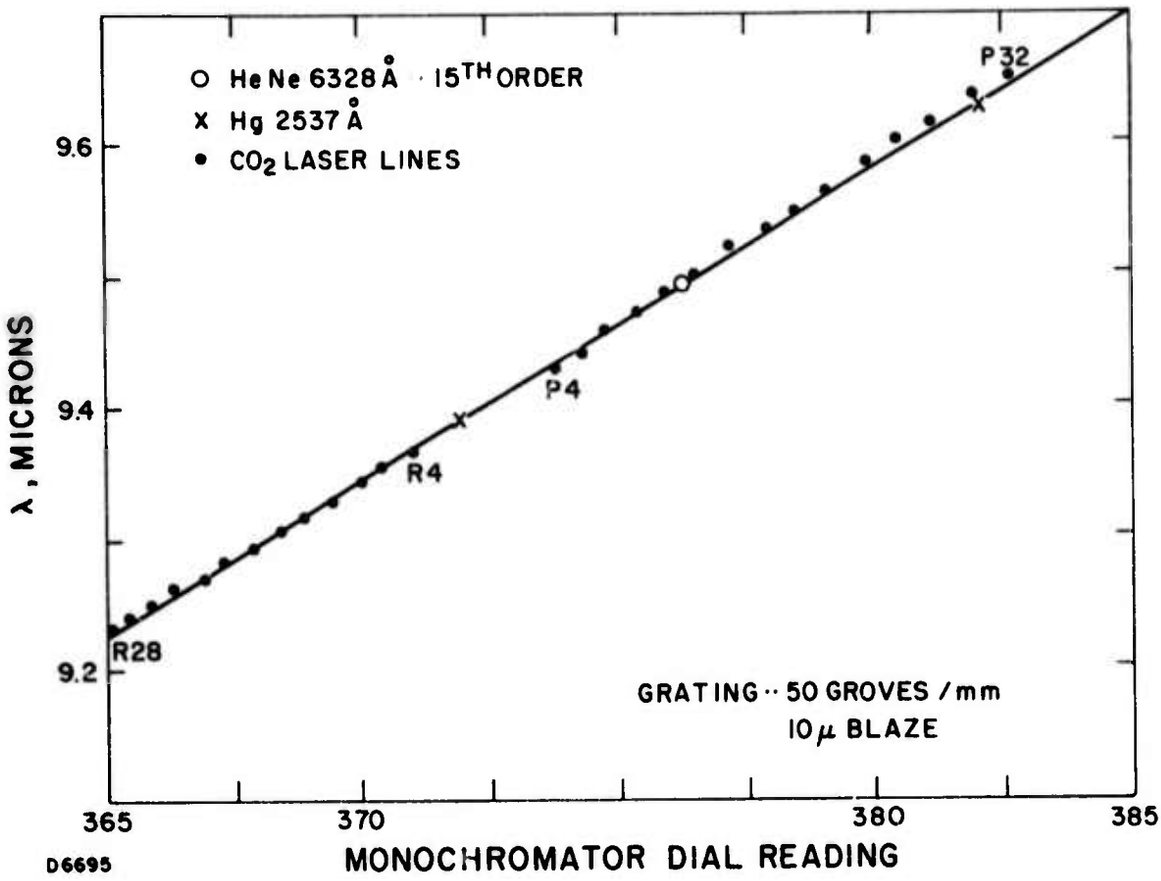

Figure 20 Monochromator Calibration. Slope of the line is fixed theoretically by knowing the monochromator geometry.

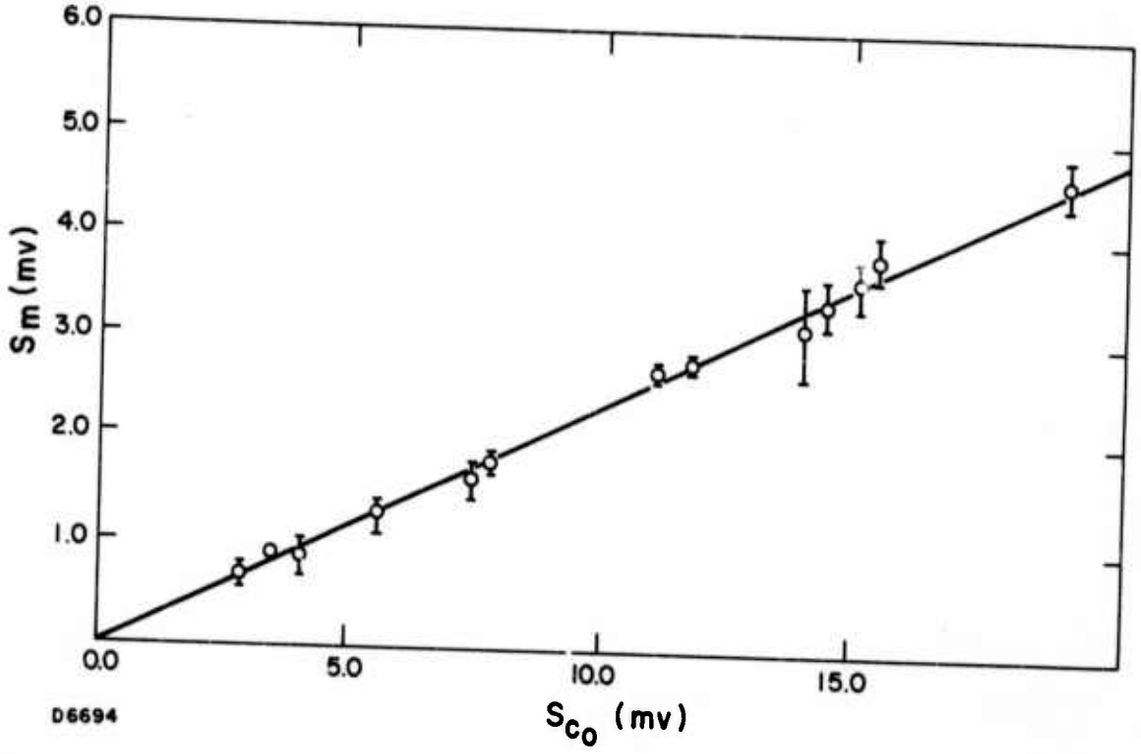

Figure 21 Relative Calibration of the Detectors D_M and D_C from their Responses S_M and S_{C_o}, Respectively, to a Varied Output from the Laser Beam.

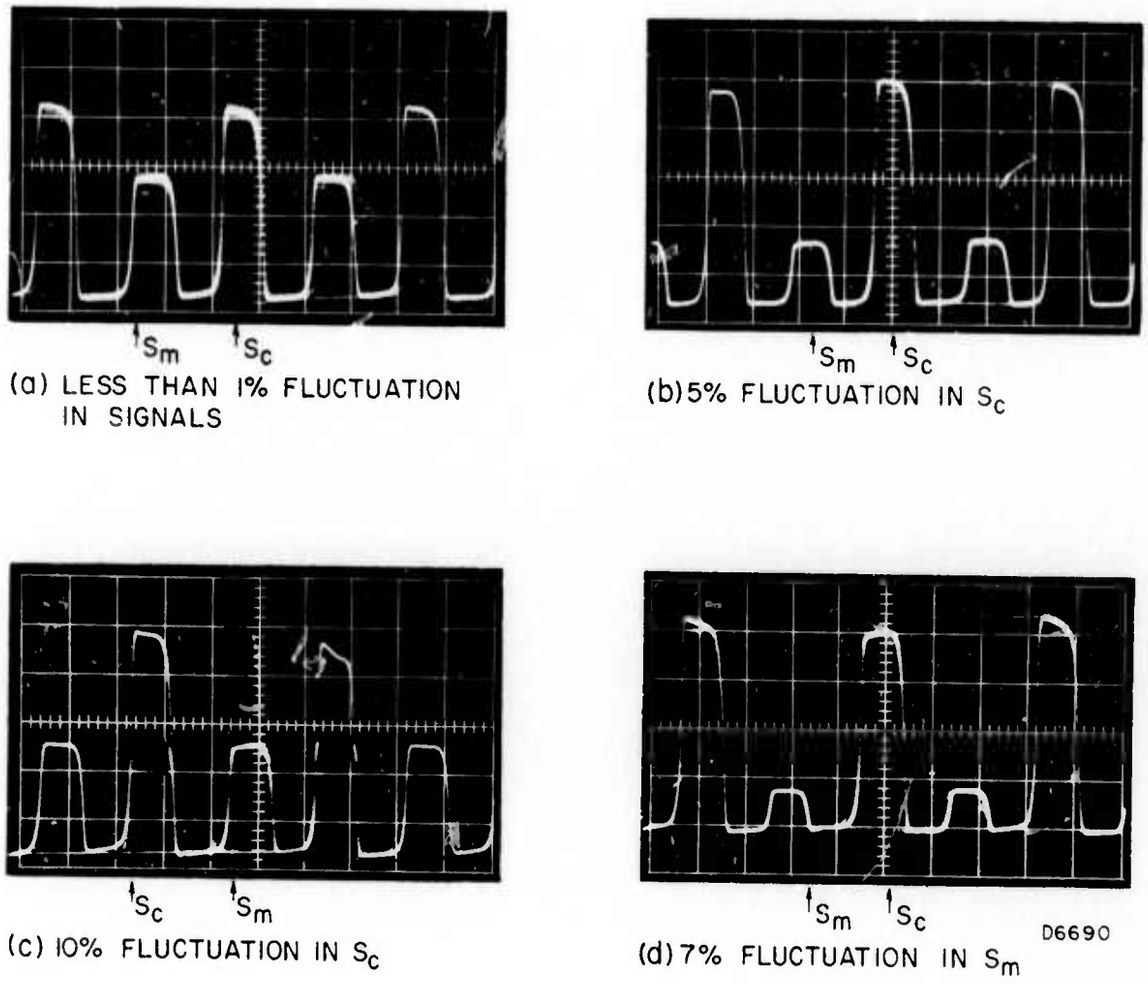

Figure 22 Oscillographs of Signals S_C and S_M: 2 mV/cm and 2 msec/cm.

The transmittance of the samples were also measured with a general laboratory spectrometer (Perkin-Elmer Model 457). The two values of the transmittances are plotted versus each other in Figure 23. The data points fall on a 45^{o} line, as they should, to within an uncertainty that is less than the uncertainty associated with the spectrometer measurements.

3.2.3 Absorption Measurements with Ozone

For the absorption measurements with ozone, the test cell was filled to approximately 4 torr with a mixture of O_2 and ozone. At this pressure the absorption lines are Doppler broadened, and the presence of O_2 is irrelevant. The total pressure was measured with a halocarbon oil manometer. The ozone concentration was determined by 2537 Å mercury line absorption. The decay time of the ozone in the test cell, presumably due to decomposition at the walls, was measured to be 280 minutes to lose 63% of an initial value. Because absorption measurements on a particular sample lasted approximately an hour, corrections for the slowly decreasing ozone concentration were made.

The transmittance of a particular CO_2 laser line by a sample was determined by the procedure previously described for CaF_2. The absorption cross section, σ_v, was determined by the equation

$$\sigma_v = - \frac{\ln I/I_o}{N_{O_3} l_c}$$

where N_{O_3} is the number density of ozone (molecules/cc) and l_c is the length of the test cell (cm). Our results for the absorption cross sections for the P-branch of the 9.6μ CO_2 transition are shown in Figure 24. Due to a procedural error the cross section for the absorption of the P26 line was not determined. For CO_2 lines P4 → P24, P_{O_3} = 2.1 and P_{O_2} = 4.4 torr, for P28 → P34, P_{O_3} = 2.5 and P_{O_2} = 3.8 torr; for P36 → P42, P_{O_3} = 1.9 and P_{O_2} = 1.7 torr.

Sources of error in making the measurements included fluctuations in the laser output and shifts in the position of the beam. Fluctuations in output on a time scale longer than the chopping period will not effect the

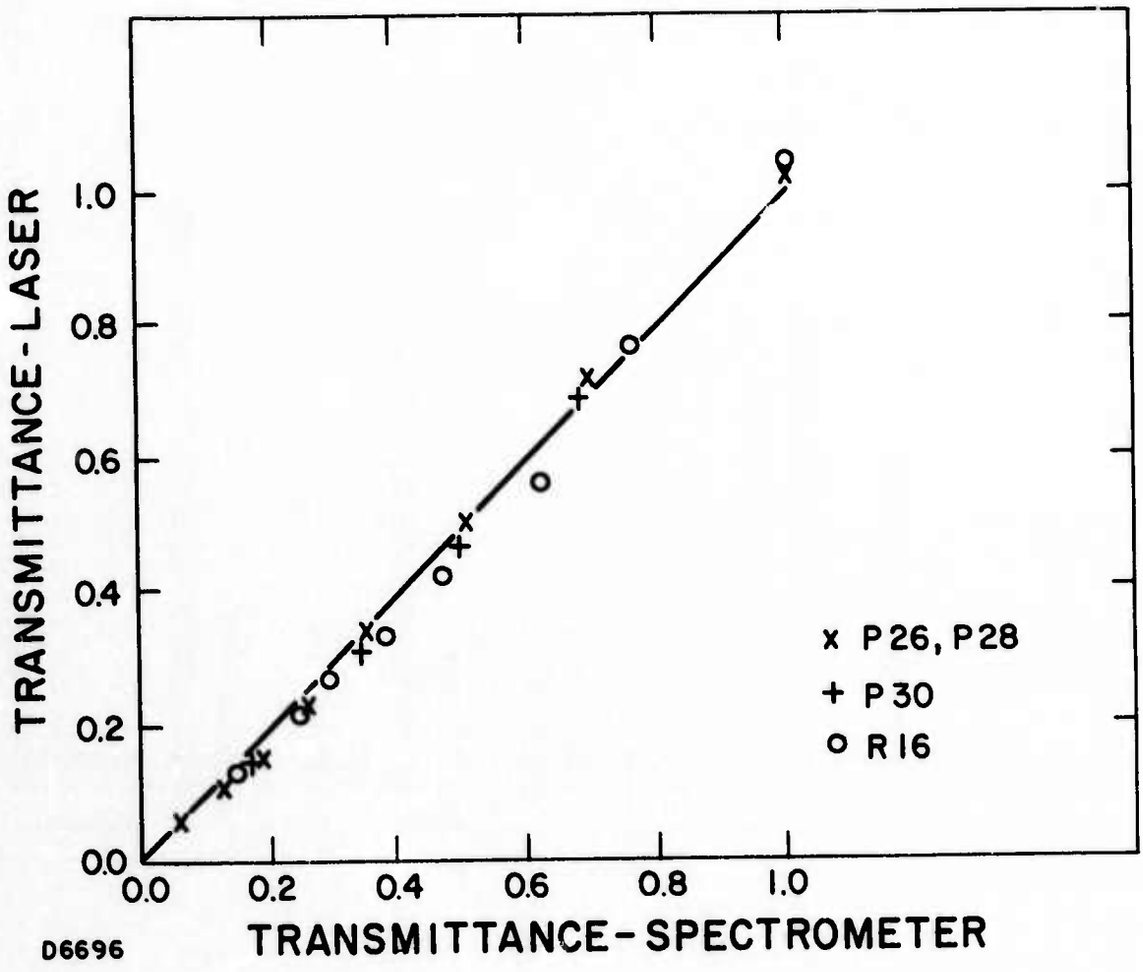

Figure 23 IR Absorption by CaF_2 as Measured by a General Laboratory Spectrometer and by the Laser/Ozone Absorption Apparatus.

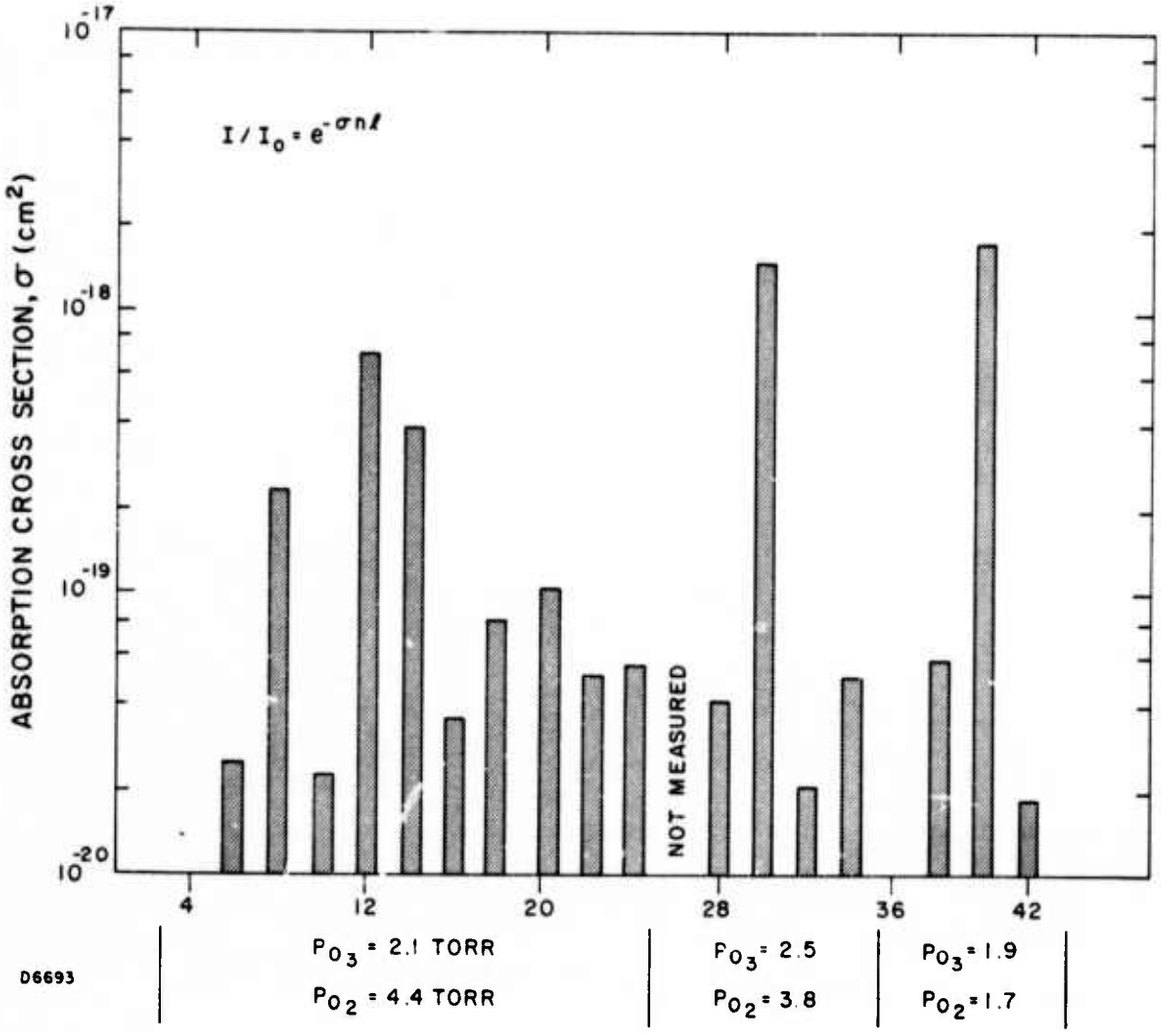

Figure 24 Cross Section for Absorption by Room Temperature, Doppler Broadened Ozone Lines of CO_2 001 → 020 P-Branch Laser Lines.

measurements. However, fluctuations have been observed on a time scale shorter than the chopping frequency as illustrated in Figure 22(b) and (c). When possible the effect of these fluctuations were minimized by averaging successive signals on the oscillograph.

Shifts in the position of the beam can result from changes in the mode structure of the beam. Closing the iris in front of the grating tended to stabilize the mode structure and reduce this as a source of error. Shifts in the position of the reflected beam were caused by misalignment of the two mirrors mounted on the chopper (Figure 22(d)). These fluctuations could be minimized by proper positioning of the detector.

An additional set of absorption measurements were made in which the ozone pressure was varied from 0.61 torr to 1.92 torr. The P30 line, a strongly absorbed line, and the P28 line, a weakly absorbed line, were tested. The results are shown in Table 1. As expected in a Doppler broadened regime, the absorption cross sections showed no systematic pressure dependence.

TABLE 1. ABSORPTION CROSS SECTIONS FOR P30 AND P28 LINES AT DIFFERENT PRESSURES

P_{O_3} (torr)	P_{O_2} (torr)	Cross Section ($cm^2 \times 10^{20}$) P30	P28
0.61	0.26	176	4.52
0.87	0.47	235	6.82
1.9	0.83	168	3.64
2.5	3.8	146	——

3.3 VIBRATIONAL RELAXATION MEASUREMENTS

To perform the laser fluorescence measurements, the apparatus was modified as shown in Figure 25. The concave mirror which decoupled the radiation from the cavity was replaced by a planar mirror mounted in a Q-switched device. The mirror was rotated at 250 cps. A new absorption cell

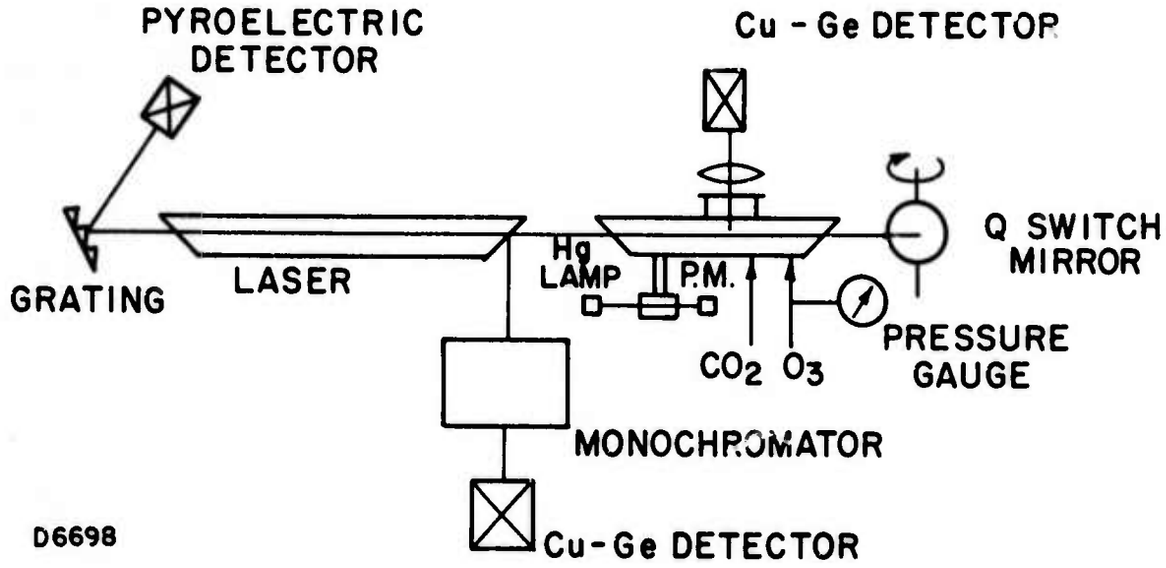

Figure 25 Experimental Configuration for Laser Fluorescence Measurements.

was mounted within the optical cavity. The cell was 11 cm in length, with BaF_2 windows fixed at the Brewster angle at each end, and a third BaF_2 window mounted on the side of the cell. Radiation partially reflected from one of the salt windows of the discharge cavity was monitored by the monochromator to determine on which transition the laser was operating. IR radiation passing through the side window of the cell was focused by an Irtran II lens onto a Cu-Ge detector. A cold (5°K) filter which passed 8 - 12μ radiation prevented stray radiation from entering the detector.

As a check on the experimental apparatus and procedures, the laser fluorescence measurement of CO_2 vibrational relaxation, as performed by Moore[35] was repeated. The Cu-Ge detector was replaced with an In-Sb detector equipped with a narrow bandpass filter which allowed observation of the 4.3μ radiation from the decay of the 001 state of CO_2. The laser was operated on a line of the P-branch of the 001 → 020 transition. The decay of the 001 state of CO_2 was recorded on an oscillograph of which Figure 26 is representative. Five measurements were made at CO_2 pressures in the range 35 to 100 torr. The average value obtained for the product of the CO_2 pressure and the decay time, $P_{CO_2} \tau_{CO_2\text{-}CO_2}$, was 3.63 atm, μsec, independent of pressure and in agreement with Moore, et al.[35]

Using the procedure previously described, the rate for deactivation of vibrationally excited CO_2 by ozone was measured. In these runs, the laser was allowed to operate on several lines of the 001 → 100 transition by replacing the grating with a flat mirror. The absorption cell was filled with a mixture of CO_2, ozone and helium. The helium was added to increase the thermal capacitance of the mixture. The measurements were made with two mixtures; the proportions of He, CO_2 and ozone being 45:6:1 and 40:16:1. Total pressures of the mixtures ranged between 13 and 380 torr.

Values of $P_{O_3} \tau_{CO_2\text{-}O_3}$ were determined from the formula

$$\frac{1}{P_{O_3} \tau_{CO_2\text{-}O_3}} = \frac{1}{\phi_{O_3}} \left[\frac{1}{(P\tau)_{mix}} - \frac{\phi_{CO_2}}{P_{CO_2} \tau_{CO_2\text{-}CO_2}} - \frac{\phi_{He}}{P_{He} \tau_{CO_2\text{-}He}} \right]$$

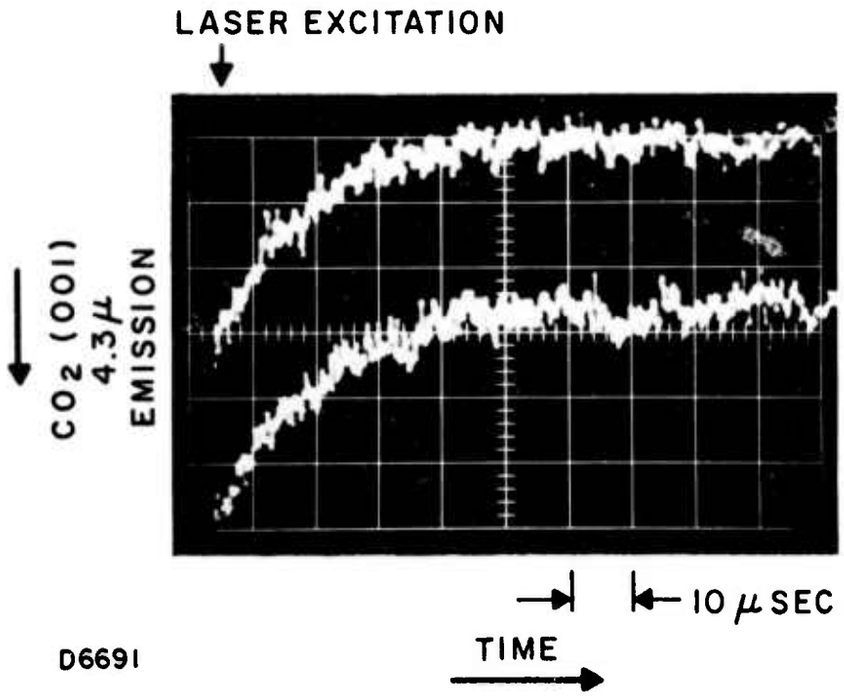

Figure 26 Oscillograph Showing Two Single Pulse Laser Fluorescence Experiments on the Decay of Vibrationally Excited CO_2 (001). P_O = 1.8 torr, p_{CO_2} = 10 torr, P_{He} = 75 torr, sweep = 10μsec/cm.

where ϕ_i is the mole fraction of the i^{th} species (i = CO_2, O_3, He) and $(P\tau_{mix})$ is the product of the mixture total pressure and the decay time for excited CO_2 as recorded on the oscillographs. In Figure 27 the values of $\tau^{-1}_{CO_2\text{-}O_3}$ are plotted vs P_{O_3}. The data points lie along a straight line passing through the origin whose slope gives $P_{O_3}\,\tau_{CO_2\text{-}O_3} = 0.0324$ atm μsec(or $k = 4.1 \times 10^4$ torr^{-1} sec^{-1}, $\sigma = 0.24$ Å^2).[43]

The fluorescence measurement of ozone vibrational relaxation is similar to that for CO_2; there are several problems however peculiar to the ozone fluorescence measurement. For the ozone measurement the fluorescence radiation is approximately the same wavelength as the laser radiation. Because of this it is much more important that the detector be shielded for both direct and scattered laser radiation. Spectral discrimination by either a narrow bandpass interference filter or a monochromator is another approach to this problem. Another problem is related to having an intracavity rather than extracavity absorption cell which by its nature alters the performance of the laser. Ozone, unlike CO_2, significantiy absorbs only a few wavelengths emitted by the CO_2 laser. It is therefore difficult to excite the ozone using a wavelength it strongly absorbs, for the neighboring laser transitions will then have much larger gains, inducing the laser to shift to these transitions.

Two procedures were followed in attempting to observe ozone fluorescence. In the first procedure the absorption cell was evacuated and the laser was operated on the P30 transition, a wavelength strongly absorbed by ozone. Ozone was then admitted into the cell in an amount which reduced the laser radiation intensity by approximately one half. At this point approximately one torr of ozone was in the cell. The pressure was then decreased in small increments until it was less than 0.01 torr. At each pressure attempts were made to observe ozone fluorescence with the Cu-Ge detector. At no time were signals observed which could be identified with vibrationally excited ozone. Since we were operating with a wide bandpass filter (8-12μ) on the detector, there was a large detector response to scattered light from the laser pulse, and it was subsequent to the recovery from this pulse that we could look for ozone fluorescence.

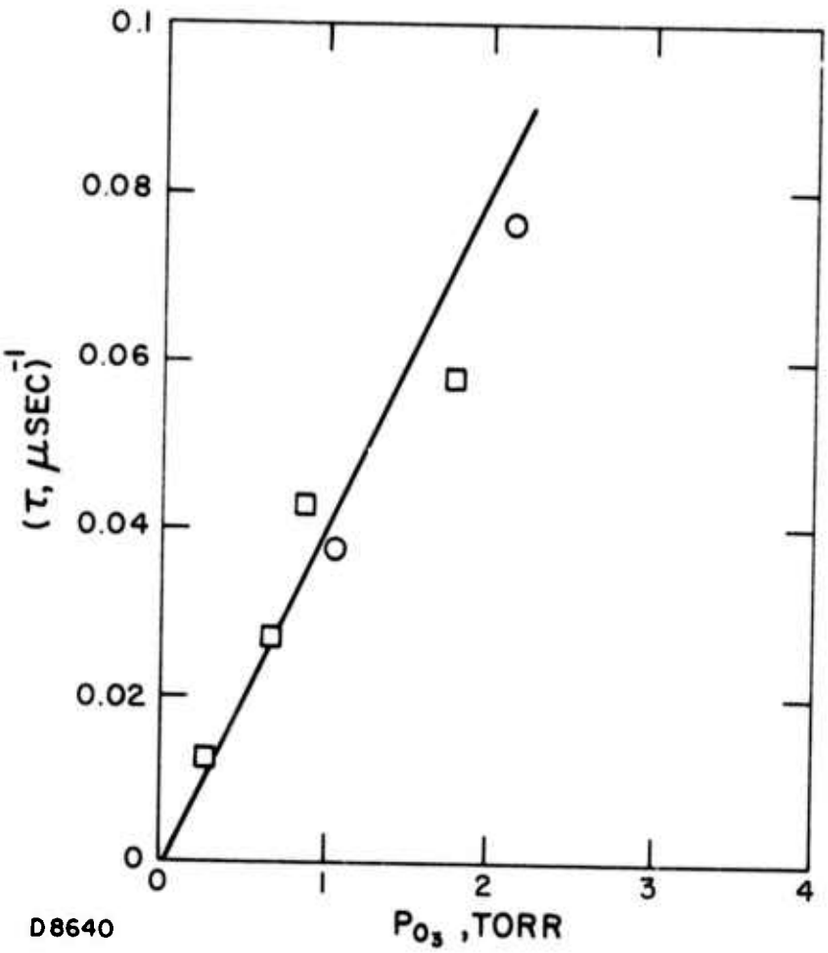

Figure 27 Reciprocal of Relaxation Time for Mixture vs P_{O_3}. He:CO_2:O_3 = 45:6:1, O; 40:16:1, □

In the second procedure, the absorption cell contained between one and 40 torr of ozone. Lasing was successively initiated on each transition of the P-branch. For several transitions however the large absorption of the ozone prevented lasing. Again no ozone fluorescence was observed.

The next step in this work should be to place the absorption cell extracavity in the same configuration for which the absorption cross section data were obtained. In this way quantitative knowledge of laser energy absorbed on a pulse can be reliably estimated and the problem of driving the laser oscillation to a non-absorbing wavelength can be prevented. Further, appropriate spectral filtering of the detector should be performed to prevent its response to the laser and allow observations closer to the moment of excitation.

REFERENCES

1. J.K. Cashion and J.C. Polanyi, Proc. Roy. Soc., A258, 529 (1960).
2. C.J. Hochanadel, J.A. Ghormley and J.W. Boyle, J. Chem. Phys. 48, 2416 (1968).
3. J.F. Riley and R.W. Cahill, J. Chem. Phys. 52, 3297 (1970).
4. P.L.T. Beran and G.R.A. Johnson, J. Chem. Soc. Faraday I 69, 216 (1973).
5. C.W. von Rosenberg, Jr. and D.W. Trainor, J. Chem. Phys. 59, 2142 (1973).
6. D.J. McCaa and J.H. Shaw, J. Mole. Spec. 25, 374 (1968).
7. J.G. Calvert and J.N. Pitts, Jr., Photochemistry (John Wiley and Sons, Inc., New York, 1966).
8. D. Biedenkapp and E.J. Bair, J. Chem. Phys. 52, 6119 (1970).
9. R. Gilpin, H.I. Schiff and K.H. Welge, J. Chem. Phys. 55, 1087 (1971).
10. D.W. McCullough and W.D. McGrath, Chem. Phys. Letters 12, 98 (1971).
11. E. Lissi and J. Heicklen, J. Photochem. 1, 39 (1972/73).
12. F. Kaufman and J.R. Kelso, J. Chem. Phys. 46, 4541 (1967).
13. M.F.R. Mulcahy and D.J. Williams, Trans. Faraday Soc. 64, 59 (1968).
14. P.D. Francis, Brit. J. Appl. Phys. 20, 1717 (1969).
15. F. Stuhl and H. Niki, J. Chem. Phys. 55, 3943 (1971).
16. S.W. Benson and A.E. Axworthy, J. Chem. Phys. 42, 2614 (1965).
17. T.P.L. Izod and R.P. Wayne, Proc. Roy. Soc. A308, 81 (1968).
18. J.F. Noxon, J. Chem. Phys. 52, 1852 (1970).
19. F. Stuhl and K. Welge, Can. J. Chem. 47, 1870 (1969).

20. L. Wallace and D. M. Hunter, J. Geophys. Res. 73, 4813 (1968).

21. R. A. Young and G. Black, J. Chem. Phys. 47, 2311 (1967).

22. I. D. Clark and R. P. Wayne, Chem. Phys. Letters 3, 93 (1969).

23. R. P. Steer, R. A. Ackerman and J. N. Pitts, Jr., J. Chem. Phys. 51, 843 (1969).

24. M. Gauthier and D. R. Snelling, Chem. Phys. Letters 5, 93, (1970).

25. R. J. McNeal and G. R. Cook, J. Chem. Phys. 47, 5387 (1967).

26. K. H. Becker, W. Groth and U. Schurath, Chem. Phys. Letters 14, 489 (1972).

27. J. L. McCrumb and F. Kaufman, J. Chem. Phys. 57, 1270 (1972).

28. R. A. Young, G. Black and T. G. Slanger, J. Chem. Phys. 49, 4758 (1968).

29. D. M. Hunten and M. B. McElroy, Rev. Geophys. 4, 303 (1966).

30. D. R. Snelling and E. J. Bair, J. Chem. Phys. 47, 228 (1967).

31. S. S. Penner, Quantitative Molecular Spectroscopy and Gas Emissivities, p. 141 (Addison-Wesley Publishing Co., Inc., Reading, MA, 1959).

32. C. E. Treanor, J. W. Rich and R. G. Rehm, J. Chem. Phys. 48, 1798 (1968).

33. K. N. C. Bray, J. Phys. B. (Proc. Phys. Soc.) 1, 705 (1968).

34. L. O. Hocker, M. A. Kovacs, C. K. Rhodes, G. W. Flynn and A. Javan, Phys. Rev. Letters 17, 233 (1966).

35. C. B. Moore, R. E. Wood, B-L. Hu and J. T. Yardley, J. Chem. Phys. 46, 4222 (1967).

36. W. A. Rosser, Jr., A. D. Wood and E. T. Gerry, J. Chem. Phys. 50, 4996 (1969).

37. N. N. Sobolev and V. V. Sokovikov, Soviet Physics Uspekhi 10, 153 (1967).

38. S. A. Clough and F. X. Kneizys, AFCRL, Physical Sciences Research Paper No. 170, "Ozone Absorption in the 9.0 Micron Region," AFCRL-65-862, Optical Physics Laboratory Project 7670, November, 1965.

39. A. Goldman, D. Murcray, F. Murcray and W. Williams, Physics Dept., University of Denver, "Atmospheric Absorption of Solar Radiation by the 9.6μ Ozone Band," prepared for AFCRL, Office of Aerospace Research, Bedford, Mass. under ARPA Order No. 363, Contract AF 19 (628)-5202 Scientific Report No. 6, October, 1967.

40. L.D. Kaplan, M.V. Migeotte and L. Neven, J. Chem. Phys. 24, 1183 (1956).

41. S.A. Clough and F.X. Kneizys, J. Chem. Phys. 44, 1855 (1966).

42. R.A. McClatchey, et al., "AFCRL Atmospheric Absorption Line Parameters Compilation," AFCRL TR-73-0096, Environmental Res. Papers No. 434 (1973).

43. C.W. von Rosenberg, Jr. and A. Lowenstein, J. Chem. Phys. 59, 2751 (1973).

APPENDIX A

QUANTITATIVE REDUCTION OF IR-SIGNALS TO OBTAIN ϕ

The reduction of the peak signal on an oscillogram to a value of ϕ involves the following procedure.

A calibration factor C is determined for the detector for each series of photolysis runs. It is obtained with the detector, its associated shielding, bias circuit, filter, lens and stack of apertures as shown in Figure 1 down to the top phenolic end plate all operating as a unit. As described in Section 2.3 a room temperature, T_r, chopper and ice temperature blackbody are used. The relation

$$S = C \int_{\Delta\lambda} D_\lambda \left[N^o_\lambda (T_r) - N^o_\lambda (273^oK) \right] d\lambda$$

is used to define C, where

- S = signal from detector, mV
- C = calibration factor, mV cm^2 ster $watt^{-1}$
- D_λ = spectral response of detector system previously determined for the particular filter in use (see Section 2.3), non-dimensional.
- N^o_λ = Planck blackbody function at temperature T and wavelength λ, watts cm^{-2} $ster^{-1}$ μ^{-1}
- $\Delta\lambda$ = spectral interval over which detector system has nonzero response, μ.

The radiating gas signal is written as

$$S_g = C \int D_\lambda R_\lambda \, d\lambda$$

$$R_\lambda = \frac{[O_3 (v=1)]}{4\pi\tau_1} \ell h\nu f_\lambda$$

Preceding page blank

where

S_g = signal from the gas (ozone), mV

R_λ = radiation from gas watts cm^{-2} $ster^{-1}$ μ^{-1}

$[O_3(v=1)]$ = number density of radiating ozone, cm^{-3}

τ_1 = radiative lifetime of ozone $v = 1 \rightarrow 0$ for the band of interest (e.g., 94 msec for the ν_3 - mode), sec.

ℓ = path length, taken as cell length between phenolic end plates, 20 cm.

$h\nu$ = average energy per photon in the band of interest, Joules

f_λ = spectral distribution function for radiating band of interest, non-dimensional and normalized so that

$$\int_0^\infty f_\lambda \, d\lambda = 1$$

thus

$$S_g = C \frac{[O_3 (v=1)]}{4\pi \tau_1} \ell h\nu \int D_\lambda f_\lambda \, d\lambda ;$$

where

$$\int D_\lambda f_\lambda \, d\lambda \simeq 0.86$$

for the ν_3-band and for the ν_2-band system this integral is 0.65. These equations are used to obtain $[O_3(v=1)]$. The concentration of initial O-atoms, $[O]_o$, is obtained from earlier obtained UV measurements relating $[O]_o$ to gas composition, pressure and flash energy (discussed in Section 3). At this point the question of ψ enters for the $(O_3 + O_2)$ data and

$$[O]_o = [O]_p (1 + \psi)$$

where $[O]_p$ is the O-atom concentration due to primary photolysis. The value

$$f \equiv \frac{[O_3(v=1)]}{[O]_o}$$

is then used to represent the data and is the quantity plotted in Figure 12, except when self-absorption is important an additional correction is included which is described below.

The value of ϕ that fits this data is obtained by using Eqs. (5) and (6) to obtain for $t = t_{max}$

$$f = \phi \frac{R}{1-R} [e^{-A} - e^{-B}] \qquad (A-1)$$

where $A = \frac{R\ell nR}{R-1}$ and $B = \frac{A}{R}$.

Equation (A-1) is also displayed in Figure 12; from its definition the quantity f is expected to basically scale linearly with pressure especially at the lower pressures where $\tau_r \gg \tau_v$ and the steady state solution is valid. This behavior is illustrated in Figure 12 by the dashed line which passes through the 200 torr value of (A-1) and sets f proportional to pressure at other points.

Self-Absorption

One important question in the interpretation of data from this experiment is the importance of self-absorption by the ozone of the ozone emission. If one does a "worst case" calculation by considering the line center absorption by the most strongly absorbing line in the ν_3-band one obtains $S = 0.363$ atm^{-1} cm^{-2} at $T = 281^oK$ and $\nu = 1065.1246$ cm^{-1}.[38] If the line width is 0.05 cm^{-1} at 1 atm due to pressure broadening, which is a reasonable guess, then for 200 torr and 0.3% ozone $k \simeq 0.02$ cm^{-1} is the absorption coefficient. The cell length including the upper non-active portion with the apertures is about 40 cm giving an attenuation of $I/I_o = e^{-0.8} = 0.45$ for this worst case. Since there is emission from many other lines where the absorption is much less, the integrated result is not clear except it is expected to be less drastic than this. Experimentally we addressed the

problem by doing a few runs with an Irtran IV window separating the upper chamber (20 cm long) with the aperture from the lower chamber (20 cm also) with the flashlamps. The peak signal, at 200 torr was 1.15 larger with the upper chamber filled with N_2 instead of 200 torr of (O_3 + O_2) mixture. The mechanism is resonant absorption of ozone emission by the undissociated ozone (at equal rotational temperature and under identical conditions of pressure broadening). Varying the pressure should not vary this absorption if O_3 is a constant fraction of the mix because the lines broaden and reduce their absorption/per molecule linearly with pressure while the number of absorbers increases linearly with pressure. Thus, a constant correction was applied to the data by multiplying f by 1 + C where C = 0.15 * 30/20 cm; the 30 cm path length used here represents the upper chamber plus 1/2 the lower chamber length and therefore represents the average distance photons must travel to reach the detector.

APPENDIX B

VARIOUS MODELS FOR RECOMBINATION/RELAXATION

Several models will be summarized here by comparing their steady state expressions for the IR signal.

The reactions that are considered are

$$O + O_2 + O_2 \xrightarrow{\phi_v k_1} O_3(v) + O_2, \quad v = 0, 1, \ldots m \tag{B-1}$$

$$O_3(v) + O_2 \xrightarrow{k_{2,v}} O_3(v-1) + O_2, \quad v = 1, 2 \ldots m \tag{B-2}$$

$$O_3(v) + O_3(v') \longrightarrow O_3(v-1) + O_3(v'+1) \qquad \begin{matrix} m \geq v \geq 1, \\ (m-1) \geq v' \geq 0 \end{matrix} \tag{B-3}$$

$$O_3(v) \xrightarrow{\tau_v} O_3(v-1) + h\nu, \quad m \geq v \geq 1 \tag{B-4}$$

In all that follows (B-4) is not considered a significant loss mechanism for vibrational quanta, rather it is simply the mechanism of the diagnostic, via IR emission.

MODEL I

If in (B-1) v = 0 and 1 only are allowed then

$$\frac{d[O_3(1)]}{dt} = R_1 \phi_1 - R_2 [O_3(1)] = 0$$

where $R_1 = k_1 [O] [O_2]^2$ and $R_2 \equiv k_2 [O_2]$ (where $k_2 \equiv k_{2,1}$) has a solution

$$[O_3(1)] = R\phi_1$$

where $R \equiv R_1/R_2$ and the signal is

$$S_I = \frac{K}{\tau_1} [O_3(1)] = \frac{K}{\tau_1} R\phi_1 \qquad \text{(B-I)}$$

where $K = C \frac{h\nu\ell}{4\pi}$ and C is defined in Appendix A.

MODEL II

If in (B-1) v takes all values and (B-3) is fast relative to (B-1) and (B-2), and there is sufficient $O_3(0)$ so that (B-3) is never at a loss for $O_3(v' = 0)$ collision partners then the V-V process will shuffle all quanta down to v = 1. This is because the Boltzmann factor $\exp(-h\nu/kT) < 10^{-2}$ for $\lambda = 10\mu$ quanta and $T = 300^{\circ}K$; i.e., one $O_3(9)$ formed in recombination will, by the V-V shuffle reaction (B-3) with no less than eight $O_3(0)$, generate nine $O_3(1)$. From this point it is clear by inspection that the signal

$$S_{II} = \frac{K}{\tau_1} R \sum_1^m v\phi_v \qquad \text{(B-II)}$$

where v = m is the maximum quantum number accessible in the recombination. The value of $k_{2,v}$ for $v > 1$ do not enter if we assume all quanta were quickly shuffled down to v = 1.

MODEL III

If in (B-1) v takes all values, $k_{2,v} = k_2$ and $\tau_v = \tau_1$ for all v, and if (B-3) is slow relative to (B-1) and (B-2) (no V-V shuffle) then the equations

$$\frac{d[O_3(0)]}{dt} = \phi_0 R_1 + [O_3(1)] R_2$$

$$\frac{d[O_3(1)]}{dt} = \phi_1 R_1 + [O_3(2)] R_2 - [O_3(1)] R_2$$

$$\frac{d\,[O_3(v)]}{dt} = \phi_v R_1 + [O_3(v+1)]\, R_2 - [O_3(v)]\, R_2$$

and

$$\frac{d\,[O_3(m)]}{dt} = \phi_m R_1 - [O_3(m)] R_2,$$

have a steady state solution found by setting all derivatives equal to zero and solving the relations in turn starting with

$$[O_3(m)] = R\phi_m,$$

and then proceeding to $v = m - 1$, etc., e.g.,

$$[O_3(m-1)] = R(\phi_m + \phi_{m-1})$$

$$[O_3(v)] = R(\phi_m + \phi_{m-1} + \ldots + \phi_v)$$

The signal is then given by

$$S_{III} = K \sum_1^m \frac{[O_3(v)]}{\tau_v} = \frac{K}{\tau_1} \sum [O_3(v)],$$

from which

$$S_{III} = \frac{K}{\tau_1} R \sum_1^m v\,\phi_v \qquad \text{(B-III)}$$

follows by inspection.

MODEL IV

If in (B-1) v takes all values, $k_{2,v} = k_2$, but $\tau_v = \tau_1/v$ and (B-3) is slow then a similar procedure yields

$$S_{IV} = \frac{K}{\tau_1} R \sum_{1}^{m} \frac{v(v+1)}{2} \phi_v \qquad \text{(B-IV)}$$

MODEL V

If we have the same assumptions as in MODEL IV except $k_{2,v} = vk_2$ then we obtain

$$S_V = \frac{K}{\tau_1} R \sum_{1}^{m} v\phi_v \qquad \text{(B-V)}$$

APPENDIX C

EQUILIBRATION WITH FAST V-V SHUFFLE

If one has a system of N harmonic oscillators with Q total quanta among them and the distribution of quanta is constrained to satisfy

$$N_v = N_o e^{-v\theta/T_v} \tag{C-1}$$

where N_v = number of the harmonic oscillators in vibrational level v (at an energy v x θ above the ground state) and T_v is the vibrational temperature then we have

$$\sum_o^M N_v = N \tag{C-2}$$

$$\sum_o^M vN_v = Q \tag{C-3}$$

where M is the maximum vibrational level allowed. These three equations give

$$\sum_o^M R^v = \frac{N}{Q}\sum_o^M vR^v, \quad R \equiv e^{-\theta/T_v} \tag{C-4}$$

which may be solved for T_v if N/Q is specified (as well as θ and M). For the ozone ν_3-mode, $\theta = 1498^oK$ and M = 8 is obtained by dividing the 1.105 eV $O\text{-}O_2$ bond strength by θ.

Examples

a) $N/Q = 1 \rightarrow R \simeq 0.5$ or $T_v \simeq 2160^oK$ ($\theta = 1498^oK_v$)

b) $N/Q = 2.3 \rightarrow R \simeq 0.3$ or $T_v = 1250^oK$

c) $N/Q = 3 \rightarrow R \simeq 0.25$ or $T_v \simeq 1080^{\circ}K$

d) $N/Q = 4 \rightarrow R \simeq 0.2$ or $T_v \simeq 930^{\circ}K$

e) $N/Q = 20 \rightarrow R \simeq 0.05$ or $T_v \simeq 500^{\circ}K$

f) $N/Q = \infty \rightarrow R = 0$ or $T_v = 0^{\circ}K$

APPENDIX D

SYNTHETIC SPECTRA

The spectral intensity in the vicinity of 10μ of ozone at $300^{\circ}K$ is shown in Figure 16(a). This was constructed by the use of a computer code and associated tape which contains the absorption coefficients of all the ozone lines that could be important in atmospheric absorption problems.[42] We* attempted to construct higher temperature (with higher T_v but $T_r = 300^{\circ}K$) spectral intensity plots from our code and the tape of lines but found that an integral over the resulting plot gave progressively (and considerably) lower values for the integrated band intensity. This is symptomatic of not including lines of the higher vibrational levels; they are not on the tape since it was assembled to deal with atmospheric absorption problems where $T \lesssim 300^{\circ}K$ is the case.

In order to get an approximate representation of ozone emission with higher T_v and $T_r = 300^{\circ}K$ as is appropriate for interpretations of our experiment we applied the following procedure:

1. Assume the ν_3 spectrum in Figure 16(a) is principally due to $\nu_3 = 1 \rightarrow 0$ transitions. This is justified by the Boltzmann factor $e^{-\Theta/T} = \exp(-1498^{\circ}/300^{\circ}K) < .007$ which implies that the population in $\nu_3 = 2$ is less than 1% of its value in $\nu_3 = 1$. Thus, we can further assume that the spectral width of the ν_3-band spectrum in Figure 16(a) is essentially due to the rotational structure of the band for $T_r = 300^{\circ}K$
2. Assume that if one desired the spectral intensity for ozone undergoing $\nu_3 = 2 \rightarrow 1$ transitions at $T_r = 300^{\circ}K$ that it would look just like Figure 16(a) except it would be shifted to longer wavelengths by 30 cm^{-1} (which is

*With assistance of L. A. Young of AERL.

based on the decrease in energy of 2-1 compared to a 1-0 transition). Assume that for $\nu_3 = n \rightarrow n-1$ the spectrum is that of Figure 16(a) except shifted to longer wavelengths by $(n-1) \times 30\ cm^{-1}$.

3. Assume that one can construct an ozone spectrum at $T_r = 300^oK$ and $T_v \neq T_r$ by a linear superposition of the Figure 16(a) spectrum where each curve in the superposition is shifted in wavelength and intensity according to the principles:

   a) The proportioning of emission between the vibrational levels is governed by populations predicted by the statistical mechanics of harmonic oscillators; i.e.,

$$\frac{N_v}{N} = \frac{e^{-v\Theta/T}}{Q}$$

   where

$$Q = (1 - e^{-\Theta/T_v})^{-1}$$

   is the partition function, N = total number density of ozone, and N_v = number density of ozone in vibration level v. The level spacing Θ, ^oK is assumed invarient with level for this part of the calculation.

   b) The integrated emission scales with the Planck blackbody function $N^o_\lambda(T)$ watts cm^{-2} $ster^{-1}$ μ^{-1}.

Thus, we construct a spectrum by application of

$$I_\lambda(T_v, T_r = 300^oK) = \frac{N^o_\lambda(T_v)}{N^o_\lambda(300^oK)} \frac{1}{Q} \left\{ I'_\lambda + I'_{\lambda - \Delta\lambda} e^{-\Theta/T_v} + I'_{\lambda - 2\Delta\lambda} e^{-2\Theta/T_v} + \ldots \right\}$$

where $I'_\lambda = I_\lambda (T_v = T_r = 300^oK)$, i.e., Figure 16(a). This spectrum is shown in Figure 16(b) for $T_v = 1250^oK$ along with the spectral response of the two detector/filter combinations of interest.